Available online at www.sciencedirect.com

ScienceDirect

Geochimica et Cosmochimica Acta 130 (2014) 93–112

Geochimica et Cosmochimica Acta

www.elsevier.com/locate/gca

Mineralogical, chemical and K–Ar isotopic changes in Kreyenhagen Shale whole rocks and <2 μm clay fractions during natural burial and hydrous-pyrolysis experimental maturation

N. Clauer [a,*], M.D. Lewan [b], M.P. Dolan [c], S. Chaudhuri [d], J.B. Curtis [e]

[a] *Laboratoire d'Hydrologie et de Géochimie de Strasbourg (CNRS/UdS), 1 rue Blessig, 67084 Strasbourg, France*
[b] *U. S. Geological Survey, Denver Federal Center, Mail Stop 977, Denver, CO 80225, USA*
[c] *Dolan Integration Group, 2520 55th Street, Suite 101, Boulder, CO 80301, USA*
[d] *Department of Geology, Kansas State University, Thompson Hall, Manhattan, KS 66506, USA*
[e] *Colorado School of Mines, Golden, CO 80401, USA*

Received 11 April 2013; accepted in revised form 9 January 2014; available online 18 January 2014

Abstract

Progressive maturation of the Eocene Kreyenhagen Shale from the San Joaquin Basin of California was studied by combining mineralogical and chemical analyses with K–Ar dating of whole rocks and <2 μm clay fractions from naturally buried samples and laboratory induced maturation by hydrous pyrolysis of an immature outcrop sample. The K–Ar age decreases from 89.9 ± 3.9 and 72.4 ± 4.2 Ma for the outcrop whole rock and its <2 μm fraction, respectively, to 29.7 ± 1.5 and 21.0 ± 0.7 Ma for the equivalent materials buried to 5167 m. The natural maturation does not produce K–Ar ages in the historical sense, but rather K/Ar ratios of relative K and radiogenic ^{40}Ar amounts resulting from a combined crystallization of authigenic and alteration of initial detrital K-bearing minerals of the rocks. The Al/K ratio of the naturally matured rocks is essentially constant for the entire depth sequence, indicating that there is no detectable variation in the crystallo-chemical organization of the K-bearing alumino-silicates with depth. No supply of K from outside of the rock volumes occurred, which indicates a closed-system behavior for it. Conversely, the content of the total organic carbon (TOC) content decreases significantly with burial, based on the progressive increasing Al/TOC ratio of the whole rocks. The initial varied mineralogy and chemistry of the rocks and their <2 μm fractions resulting from differences in detrital sources and depositional settings give scattered results that homogenize progressively during burial due to increased authigenesis, and concomitant increased alteration of the detrital material.

Hydrous pyrolysis was intended to alleviate the problem of mineral and chemical variations in initially deposited rocks of naturally matured sequences. However, experiments on aliquots from thermally immature Kreyenhagen Shale outcrop sample did not mimic the results from naturally buried samples. Experiments conducted for 72 h at temperatures from 270 to 365 °C did not induce significant changes at temperatures above 310 °C in the mineralogical composition and K–Ar ages of the rock and <2 μm fraction. The K–Ar ages of the <2 μm fraction range from 72.4 ± 4.2 Ma in the outcrop sample to 62.4 ± 3.4 Ma in the sample heated the most at 365 °C for 216 h. This slight decrease in age outlines some loss of radiogenic ^{40}Ar, together with losses of organic matter as oil, gas, and aqueous organic species.

Large amounts of smectite layers in the illite–smectite mixed layers of the pyrolyzed outcrop <2 μm fraction remain during thermal experiments, especially above 310 °C. With no illitization detected above 310 °C, smectite appears to have inhibited rather than promoted generation of expelled oil from decomposition of bitumen. This hindrance is interpreted to result from

* Corresponding author. Tel.: +33 390 24 04 33; cell: +33 680 01 80 49; fax: +33 390 24 04 02.
E-mail address: nclauer@unistra.fr (N. Clauer).

0016-7037/$ - see front matter
http://dx.doi.org/10.1016/j.gca.2014.01.007

bitumen impregnating the smectite interlayer sites and rock matrix. Bitumen remains in the <2 μm fraction despite leaching with H_2O_2. Its presence in the smectite interlayers is apparent by the inability of the clay fraction to fully expand or collapse once bitumen generation from the thermal decomposition of the kerogen is completed, and by almost invariable K–Ar ages confirming for the lack of any K supply and/or radiogenic ^{40}Ar removal. This suggests that once bitumen impregnates the porosity of a progressively maturing source rock, the pore system is no longer wetted by water and smectite to illite conversion ceases. Experimental attempts to evaluate the smectite conversion to illite should preferentially use low-TOC rocks to avoid inhibition of the reaction by bitumen impregnation.

1. INTRODUCTION

Clay minerals and particularly smectite have been suggested to act as catalysts in petroleum formation (Johns, 1979; Goldstein, 1983). Isotopic dating of smectite conversion to the less catalytically active illite may as a result be relevant to evaluate the timing of petroleum expulsion from source rocks. However, although clay minerals have recognized catalytic properties that can influence petroleum products in natural environments (Clementz, 1976; Czarnecka and Gillott, 1980; Pinnavaia, 1983), experimental pyrolysis experiments have also shown smectite to inhibit or alter petroleum generation (Espitalié et al., 1980; Tannenbaum et al., 1986). For instance, in studying the Eocene Kreyenhagen Shale of California by hydrous-pyrolysis experiments, Lewan and Whitney (1993) noticed that the expelled oil yield from this indurated source rock was 80% less than yields obtained from smectite-poor source rocks, and isolated kerogen under the same hydrous pyrolysis conditions.

The present study examines the smectite to illite conversion in the Eocene Kreyenhagen Shale, which has been shown to be an effective oil-prone source rock in the San Joaquin Basin of California (Peters et al., 1994; Lillis and Magoon, 2007). Examination of the conversion is based on K–Ar dating that is widely recognized as a reliable indicator of the progressive diagenesis (e.g., Clauer and Chaudhuri, 1995; Clauer and Lerman, 2012; Clauer, 2013), along with mineralogical and chemical changes in naturally and experimentally matured whole-rock samples and <2 μm fractions. The naturally matured sequence ranges from immature outcrop to a 5-km subsurface depth. The sample set is unique in that it evaluates the mineralogical, chemical and isotopic changes of the same rock unit subjected to progressive thermal maturity. This is in contrast to previous studies of vertical well profiles that represent samples increasing in depositional age with depth (e.g., Weaver and Wampler, 1970; Aronson and Hower, 1976), which enhances the likelihood of different starting compositions because of changing provenance and/or deposition conditions. This concern is lessened in examining the same rock unit, keeping in mind that even limited changes in provenance and depositional conditions cannot be excluded at a regional sampling scale. Experimentally matured aliquots of the same immature outcrop sample as conducted in this study alleviate this concern. However, it does introduce the issue of conducting experiments at higher temperatures to ensure experimental results in reasonable times compared to the lower temperatures and longer durations experienced in natural maturation.

Therefore, integration of observations from both natural and experimental maturation as presented here represents a potentially viable approach not previously employed in the investigations of clay-mineral diagenesis. Application of the K–Ar method as an indicator of the smectite to illite conversion appears appropriate and relevant because the changes towards complete illitization are not only visualized by potential increases of the K content, but also by variable contents of the radiogenic ^{40}Ar. Illitization of an illite–smectite mixed layer results in a significant supply of K relative to a limited increase of radiogenic ^{40}Ar resulting only from decay of ^{40}K accumulated in the mineral structure since deposition. Consequently, there is a decrease of the K–Ar ages, whereas concomitant increase of both K and radiogenic ^{40}Ar indicates the presence of detrital illite particles that contained excess of radiogenic ^{40}Ar relative to the depositional time. In addition, this study is the first, to the best of our knowledge, to evaluate K–Ar ages of experimentally matured source rocks and their <2 μm clay-rich size fraction and compare the data with those of naturally matured equivalents.

2. MATERIALS AND PROCEDURES

2.1. Sample description

The starting N1 sample used in the hydrous-pyrolysis experiments is from the Skunk Hollow outcrop located north of Coalinga, California, on the western side of the San Joaquin Basin (Fig. 1). The sample was collected from the unweathered part of the outcrop below the overlying discolored saprolite horizon. The unweathered character of the sample was verified petrographically by the presence of well-developed pyrite (Lewan, 1980). The rock has a total organic (TOC) content of 9.4 wt% with a Rock-Eval hydrogen index (HI) of 258 mg/g TOC and a temperature at maximum generation (T_{max}) of 407 °C. Elemental analyses of its isolated kerogen indicate that it is an immature Type-II kerogen with an atomic H/C ratio of 1.13 and an atomic O/C ratio of 0.22. This sample was crushed to 0.5–2.0 cm chips and thoroughly mixed to ensure homogeneity, from which aliquots were taken for each pyrolysis experiment.

The naturally matured samples are from five wells on the western side of the San Joaquin Basin (B to F in Fig. 1) as described by Dolan (1998). Seven samples were taken from cores at depths between 2585 and 2828 m in the Chevron 341-11p well. Cutting samples were collected from depths of 3218 m in the Superior SPL 48-23 well, 4093 m in Standard H-B 313 well, 4377 m in the Tenneco Schutte #1 well,

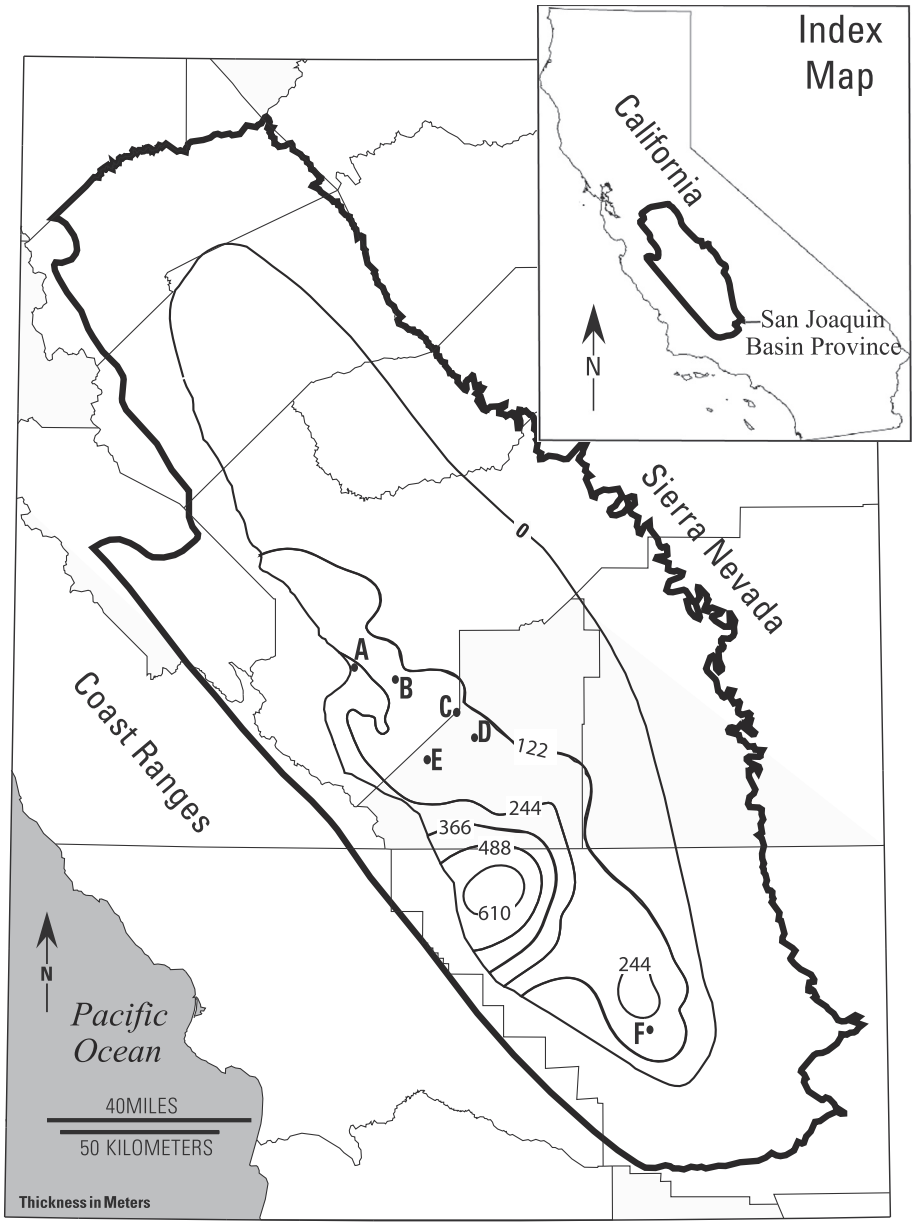

Fig. 1. Isopach map of the Kreyenhagen Shale in the San Joaquin Basin of California (modified after Peters et al., 2007b) and locations of A, Skunk Hollow Outcrop (N1 sample); B, Superior SPL 48-23 well (N9 sample); C, Standard H-B 313 well, (N10 sample); D, Tenneco-Schutte #1 well (N11 sample); E, Chevron 341-11p well, (N2 to N8 samples); and F, Arco CLA 67-29 well (N12 and N13 samples). Isopach contours represent thickness in meters for the Kreyenhagen Shale according to Peters et al. (2007b).

and 5027 and 5167 m in the Arco CLA 67-29 well. The well cutting samples were wet sieved using distilled water and a 1 mm sieve. The resulting >1 mm fraction was dried at room temperature. The samples represent a full-depth and thermal-maturity range in the San Joaquin Basin from the N1 outcrop sample in the north to the deepest well samples in the south. Although considerable changes in thickness of the Kreyenhagen Shale are reported in the San Joaquin Basin (from 34 to 686 m; Fig. 1), the collected samples occur on or between the 122- and 244-m isopach contours as mapped by Peters et al. (2007a). Noteworthy is also the fact that the geologic information was used to construct a 4-D model (Peters et al., 2007b) that does not mention abnormal conditions for the thermal burial-induced maturation and oil generation of the Kreyenhagen Shale. Its age is considered to be within the Refugian stage of the Eocene (~41–37 Ma; Johnson and Graham, 2007).

2.2. Experimental procedure

Hydrous-pyrolysis experiments were conducted in accordance with Lewan (1993) in which aliquots of the N1 crushed whole rock were heated in the presence of liquid water. Each experiment involved a 377-g aliquot of the N1

rock that was loaded into a 1-L stainless-steel (SS-316) reactor with 297 g of distilled water. These proportions of reactor volume, water, and rock, ensured that the rock was in contact with liquid water before, during, and after the experiments. After evacuating the loaded reactor, its headspace was filled with 7 MPa of helium and checked for leaks. The helium pressure was then reduced to 241 kPa, and the reactors were isothermally heated after an average initial heat-up time of 105 min to 270, 290, 310, 330, 349 and 365 °C for 72 h. In accordance with other hydrous pyrolysis experiments (Lewan, 1993), these conditions represent the full range of petroleum generation including kerogen decomposition to bitumen and bitumen decomposition to immiscible oil. One additional experiment was conducted at 365 °C for 216 h to simulate high thermal maturities beyond oil formation. After the reactors cooled to room temperatures, the generated gas, expelled immiscible oil, reacted water, and spent shale were collected as described by Lewan (1993). Spent rock was recovered after vacuum drying at 60 °C for 18 h. The spent rock aliquots and their <2 μm fractions that were separated afterwards were subjected to the same X-ray diffraction, chemical, and isotopic analyses as the original unheated N1 rock and its <2 μm fraction.

2.3. X-ray diffraction analysis

Two separate aliquots of the naturally and experimentally matured samples were gently crushed in an agate mortar. One aliquot was used for chemical analyses and K–Ar isotope determinations of the rocks and the other aliquot was dispersed in deionized water for separation of the <2 μm fraction by sedimentation following Stokes' law. The naturally and experimentally matured rocks and their <2 μm fractions were analyzed by X-ray diffraction (XRD). The determinations were made on powder mounts of the rocks, and on smear slides of the <2 μm fractions after air-drying (AD), ethylene-glycolation (EG) for 12 h, and heating (H) at 490 °C for 2 h. The illite crystallinity index (ICI) was determined on the <2 μm fractions by measuring the full width at half maximum (FWHM) height of the illite d_{001} XRD peak. This index is known to record the limited changes in the illite structural organization due to either natural burial or pyrolysis heating (e.g., Kübler and Goy-Eggenberger, 2001). Identification of illite–smectite mixed layer (I–S) is based on the absence of the d_{003} peak on the AD and EG patterns, as well as on the shape and displacement of the d_{002} peak between 8 and 4°2θ. The Reichweite, which represents the ordering of the I–S, was also determined by the precise position of the reflection between 5 and 8.5°2θ (Moore and Reynolds, 1997).

2.4. Chemical analysis

Selected major elements were determined by inductively coupled plasma-atomic emission spectrometry (ICP-AES) and inductively coupled plasma-mass spectrometry (ICP-MS) following Samuel et al. (1985) after either a tri-acid dissolution for analysis of the major, trace and rare-earth elements, or the tetraborate fusion technique for determination of K. The rocks and their <2 μm fractions were analyzed in sequence with a standard mineral (BEN-1 or GL-O) for each set of samples, to identify and reduce the analytical shifts of the equipment to improve the analytical accuracy and internal reproducibility. The outcrop N1 rock and its <2 μm fraction were also duplicated by two independent analytical sequences to consolidate the external reproducibility. Therefore, elemental variations larger than the analytical uncertainty are not attributed to analytical artifacts. The SiO_2 content could not be determined directly because Si was volatized as SiF in the tri-acid procedure. The routine precision was ±2.5% at the 2σ level, which was confirmed by the duplicate analysis of the N1 whole rock and its <2 μm fraction. The loss on ignition (LOI) was determined on some whole rocks that had sufficient left over powder after the other chemical and isotopic analyses were completed. The chemical compositions of the naturally matured rocks and <2 μm fractions were expected to be heterogeneous because of regional variable mineral compositions in the original samples prior to differential burial-induced alteration with some minerals being altered and others crystallizing at the same time. This mineral and chemical heterogeneity was not expected in the pyrolysis experiments because aliquots of the same whole rock were used in all of the experiments. This situation encouraged us to quantify the potential mineralogical and geochemical changes using Al as the conservative reference element in the natural matured and pyrolyzed rocks and their <2 μm fractions. This comparison holds only for the Al-bearing minerals, excluding the carbonates, oxides and other minor minerals, especially in the case of the whole rocks. With a routine analytical uncertainty of +3%, only the elemental ratios differing by at least 6% were considered to be significant and discussed.

2.5. K–Ar analysis

The K–Ar determinations were made on the whole rocks and <2 μm fractions of the naturally matured and experimentally pyrolyzed samples, following the protocol of Bonhomme et al. (1975). Prior to Ar extraction, the samples were heated at 80 °C under vacuum to remove the atmospheric Ar adsorbed onto the particles during preparation and handling. The blank of the extraction line and the mass spectrometer was also determined before each Ar extraction for analytical reproducibility. The amount of residual ^{40}Ar was systematically below 1×10^{-8} cm^3, which is about two orders of magnitude below the measured amounts of ^{40}Ar in the samples. The analytical accuracy and reproducibility were controlled by measuring the international standard mineral GL-O. During the course of the study, this standard averaged 24.62 ± 0.15 (2σ) $\times 10^{-6} cm^3/g$ at standard temperature and pressure (STP) of radiogenic ^{40}Ar for 5 independent measurements, and the atmospheric $^{40}Ar/^{36}Ar$ ratio averaged 294.2 ± 2.3 (2σ) for 8 independent determinations. The recommended value for the GL-O standard is $24.85 \pm 0.24 \times 10^{-6}$ cm^3/g (Odin et al., 1982), and that of the atmospheric $^{40}Ar/^{36}Ar$ ratio is close to 298.6 ± 0.4 (Lee et al., 2006). As the obtained results were internally

consistent and close to the theoretical values, no corrections were applied to the isotopic determinations. The K–Ar ages were calculated with the usual decay constants (Steiger and Jäger, 1977), with an overall analytical precision of better than ±2%.

3. RESULTS

3.1. Natural maturation

3.1.1. Whole rocks

The XRD analysis of the naturally matured whole rocks shows a classical mineral assemblage for shales with quartz, plagioclase, K-feldspar, I–S, kaolinite, carbonate(s), mica/illite, pyrite, and opal-CT, which has a broad d_{101} peak at 4.09 Å (Elzea et al., 1994). A precise quantitative evaluation of these mineral compositions was not attempted, as mineral variations were expected with varying detrital origin, alteration state, and depositional setting. However, the Al/M elemental ratios of the other analyzed major elements (labeled M) were calculated to visualize the chemical variations of the Al-bearing minerals, particularly those bearing K (i.e., feldspars, micas and clays), as a function of natural burial or experimental maturity.

The chemical compositions of the naturally matured rocks including the outcrop N1 sample show total amounts of the selected major elements (Al, Mg, Ca, Fe, Mn, Ti, Na and K) that range from 120 to 231 mg/g (Table 1). The contents of Al, Fe, Ti, Na and K generally increase with depth, whereas the limited LOI values decrease irregularly from about 18.9 to 7.42 wt%, with a high value of 21.3% for the sample at 4377 m. These combined trends suggest that the deeper samples contain more feldspars, micas and probably rutile in progressively less rock volume. Mg and Ca show no systematic changes with depth, which probably reflects a variable occurrence of carbonates. Ca has an especially wide range of concentrations. The Al/Mg, Al/Ca, Al/Na ratios are also widely scattered, whereas others such as Al/Fe remain about constant except for the N8 rock at 2828 m, which also has an abnormally high Fe content. The Al/K ratio is of special interest here as total K includes ^{40}K, which is the parent nuclide in the K–Ar dating measurements. The irregular Al/K ratio decreases from 5.75 to 4.26, except for the 6.78 value of the N3 sample at 2664 m (Table 1), probably reflecting differences in the initial mineralogy and organic matter contents of the samples. The Ti/Al ratio is also noteworthy, as Ti is often considered an immobile element insensitive to alteration. Here this ratio is quite constant, especially below 2761 m (sample N6), suggesting lack of a visible alteration of the alumino-silicate minerals, including the clay material. The large scatter of element contents and the correlatively varied Al/M ratios confirm that the rock samples had different starting mineralogical and chemical compositions. Conversely, the Al/TOC ratio increases with depth, but with some notable scatter (e.g., samples N3, N8 and N10). This increase is attributed in part to expulsion of generated oil and gas during thermal maturation. TOC losses from a source rock at the end of oil generation being of about 50% (Baskin, 1997), the decrease in TOC contents with depth greatly

Table 1
Chemical analysis of selected elements (M), total organic carbon (TOC), and Al/M ratios of naturally matured whole rocks

Sample designation	Well identification	Subsurface depth (m)	mg/g rock									LOI* (wt%)	TOC** (wt%)	Elemental ratios					
			Al	Mg	Ca	Fe	Mn	Ti	Na	K	Total			Al/Mg	Al/Ca	Al/Fe	Al/Ti	Al/Na	Al/K	Al/TOC
N1	Outcrop	0	60.8	9.91	2.45	27.5	0.223	2.99	5.60	10.9	120.4	18.9	9.4	6.13	24.8	2.21	20.3	10.9	5.58	6.47
N2	Chevron 341-11p	2585	73.0	7.10	23.0	34.4	0.258	2.69	7.30	12.7	160.4	nd	2.8	10.3	3.17	2.12	27.1	10.0	5.75	26.1
N3	Id	2664	47.8	5.59	21.0	24.3	0.140	1.90	4.50	7.05	112.3	nd	2.4	8.55	2.28	1.94	25.2	10.6	6.78	19.9
N4	Id	2676	59.3	10.3	60.8	30.6	0.310	2.55	7.72	12.7	184.3	nd	3.2	5.76	0.98	1.94	23.3	7.68	4.67	18.5
N5	Id	2719	82.8	9.65	51.2	40.7	0.325	2.55	8.36	15.5	211.1	nd	3.5	8.58	1.62	2.03	32.5	9.90	5.34	23.7
N6	Id	2761	64.6	8.29	7.66	28.3	0.133	2.94	9.00	13.0	133.9	nd	3.8	7.79	8.43	2.28	22.0	7.18	4.97	17.0
N7	Id	2786	94.5	10.3	5.44	35.7	0.214	4.17	12.3	18.5	181.1	nd	4.2	9.17	17.4	2.65	22.7	7.68	5.11	22.5
N8	Id	2828	61.8	26.6	20.0	98.0	0.624	2.77	6.27	14.5	230.6	nd	3.2	2.32	3.09	0.63	22.3	9.86	4.26	19.3
N9	Superior SPL 48-23	3218	95.8	12.4	9.68	41.7	0.288	4.48	18.7	19.5	202.5	9.7	2.2	7.73	9.90	2.30	21.4	5.12	4.91	43.6
N10	Standard H-B 313	4093	87.1	12.3	18.2	47.0	0.402	3.98	17.6	18.3	204.9	15.0	6.3	7.08	4.79	1.85	21.9	4.98	4.76	13.8
N11	Tenneco Schuttle #1	4377	99.9	11.9	9.44	48.0	0.295	4.59	14.9	19.4	208.4	21.3	2.4	8.39	10.6	2.08	21.8	6.70	5.15	41.6
N12	Arco CLA 67-29	5027	85.3	14.3	22.4	42.6	0.542	4.01	15.5	19.5	204.2	7.2	1.1	5.97	3.81	2.00	21.3	5.50	4.37	77.6
N13	Id	5167	107.0	12.6	9.27	46.4	0.244	4.99	12.2	24.8	217.5	7.4	1.3	8.49	11.5	2.31	21.4	8.77	4.31	82.3

* LOI stands for loss of ignition and nd for not determined.
** The Rock-Eval total organic carbon is from Dolan (1998), except sample N1 from USGS.

exceeds this amount of loss in the present case (Table 1), suggesting that the original rocks did not all have the same TOC content. For instance, the deepest and most thermally mature N13 sample has a TOC of 1.3 wt%. If 50% of its TOC were lost because of oil and gas expulsion, its original TOC would only be of 2.6 wt%. This calculated original value is 3.6 times less than that of the outcrop N1 sample. In addition to original differences in the amount of TOC in the samples, significant variations in the type of original organic matter are also indicated by the wide variations in $\delta^{13}C$ values (−25.2‰ to −28.3‰ V-PDB) of the isolated kerogen (Dolan, 1998). $\delta^{13}C$ values of isolated kerogen have been shown to remain essentially constant in pyrolysis experiments (±0.2‰; Lewan, 1983) and in natural maturation through metamorphism (Landergren, 1955; Gavelin, 1957). Therefore, similar to the mineralogy and chemistry of these progressively buried rocks, the initial amount and type of organic matter were significantly different as well.

The K–Ar ages of the progressively buried rocks decrease from 89.9 ± 3.9 Ma for the outcrop N1 sample to 29.7 ± 1.5 Ma for the N13 sample at 5167 m (Table 2; Fig. 2). The ages for the outcrop N1 sample and samples buried to 3218 m are significantly older than the depositional age of the unit (Refugian stage, ~41–37 Ma; Johnson and Graham, 2007), as has been often reported in the literature for such K–Ar determinations since Aronson and Hower (1976). This topic was, for instance, discussed in several easily accessible publications (e.g., Clauer and Chaudhuri, 1995; Lerman et al., 2007; Clauer and Lerman, 2012). Older ages are expected because all constitutive K-bearing minerals are detrital in origin and are mostly pristine, while they become progressively younger during burial, especially below 3220 m due to increasing mineral authigenesis and concomitant alteration of the initial K-bearing minerals (Fig. 2C).

The decrease with depth in the radiogenic ^{40}Ar content of the whole rocks is interrupted by scattered data in the 2664- to 2828-m depth range (Fig. 2B). As a result, the K–Ar ages decrease with depth from about 90 to 30 Ma, with a slight increase in the 2664- to 2828-m interval. This increase in the K–Ar age relates mainly to the scatter in K and radiogenic ^{40}Ar that vary significantly in this depth range, reflecting the already identified variable initial mineral composition. The plot of the K and radiogenic ^{40}Ar in a Harper (1970) diagram (Fig. 3A) shows that data points of the samples at and above 2786 m (i.e., sample N7) plot along a line with a zero intercept for the initial values of both coordinates. This line is considered to represent the locus of the data points for samples containing radiogenic ^{40}Ar that formed exclusively from K present in the rock. In other words, all of these rocks contain K-bearing minerals of the same origin with an average age close to 72.9 ± 2.5 Ma, and no radiogenic ^{40}Ar in excess. The exception is the outcrop N1 sample with an older age of 89.9 ± 3.9 Ma (Table 2). Below 2786 m, the relationship between K and radiogenic ^{40}Ar contents changes with the data points moving away from the equilibrium line; the resulting younger ages imply differentiated alteration in the rocks. The K–Ar age of the deepest N13 rock reports the greatest change that occurred to the rocks, despite the decay of K into radiogenic ^{40}Ar of the initial K-bearing minerals. This trend away from initial equilibrium results from an increase in K (from 1.2 to 3.3 wt%), and a decrease in radiogenic ^{40}Ar (from 8 to 3×10^{-6} cm^3/g) in the K-bearing minerals. Studying K–Ar ages of whole rocks that are progressively buried is generally considered to not be very informative for geochronological purposes, because of compositional variations in the constitutive detrital minerals. However, it can be seen here that the rocks above 2800-m depth contain K- bearing minerals that are of the same origin with about the same K–Ar age, and that below this depth the K–Ar ages progressively decrease. As expected from available studies, the K–Ar isotopic budget of the rocks includes an increasing K content and decreasing radiogenic ^{40}Ar content with increasing burial.

Table 2
K–Ar data on naturally matured whole rocks and their <2 μm fractions.

Sample designation	Subsurface depth (m)	Whole rock				<2 μm fraction			
		K_2O (wt%)	rad. Ar (%)	^{40}Ar rad. (10^{-6} cm^3/g)	Age (Ma) (±2σ)	K_2O (wt%)	rad. Ar (%)	^{40}Ar rad. (10^{-6} cm^3/g)	Age (Ma) (±2σ)
N1	0	1.45	29.98	4.31	89.9 (3.9)	1.13	18.31	2.69	72.4 (4.2)
N2	2585	1.78	49.92	4.10	70.1 (2.9)	1.43	24.15	2.86	60.9 (3.0)
N3	2664	1.02	50.26	2.43	72.6 (5.2)	1.12	28.09	2.84	77.0 (3.6)
N4	2676	1.65	63.53	4.01	73.8 (3.0)	1.49	27.09	3.04	62.2 (3.0)
N5	2719	2.07	63.59	4.98	73.1 (2.7)	1.57	24.44	3.87	75.0 (3.8)
N6	2761	1.76	54.08	4.55	78.4 (3.5)	1.17	40.21	2.59	67.4 (3.5)
N7	2786	2.40	41.07	5.90	74.8 (3.3)	1.90	26.50	4.18	67.0 (3.0)
N8	2828	1.91	59.33	3.99	63.7 (2.6)	2.09	36.47	4.43	64.7 (2.8)
N9	3218	2.57	50.60	2.79	33.4 (1.5)	2.15	50.35	2.94	41.9 (2.8)
N10	4093	2.37	71.76	3.55	45.9 (1.5)	1.88	42.57	3.49	56.7 (2.3)
N11	4377	2.62	53.88	3.19	37.3 (1.5)	1.94	48.30	3.41	53.7 (2.3)
N12	5027	2.48	55.70	2.98	36.9 (1.5)	3.52	42.09	3.49	30.5 (1.5)
N13	5167	3.15	39.94	3.04	29.7 (1.5)	4.77	46.47	3.16	20.4 (1.0)
Duplicate						4.64	46.57	3.16	21.0 (0.7)

rad. stands for radiogenic.

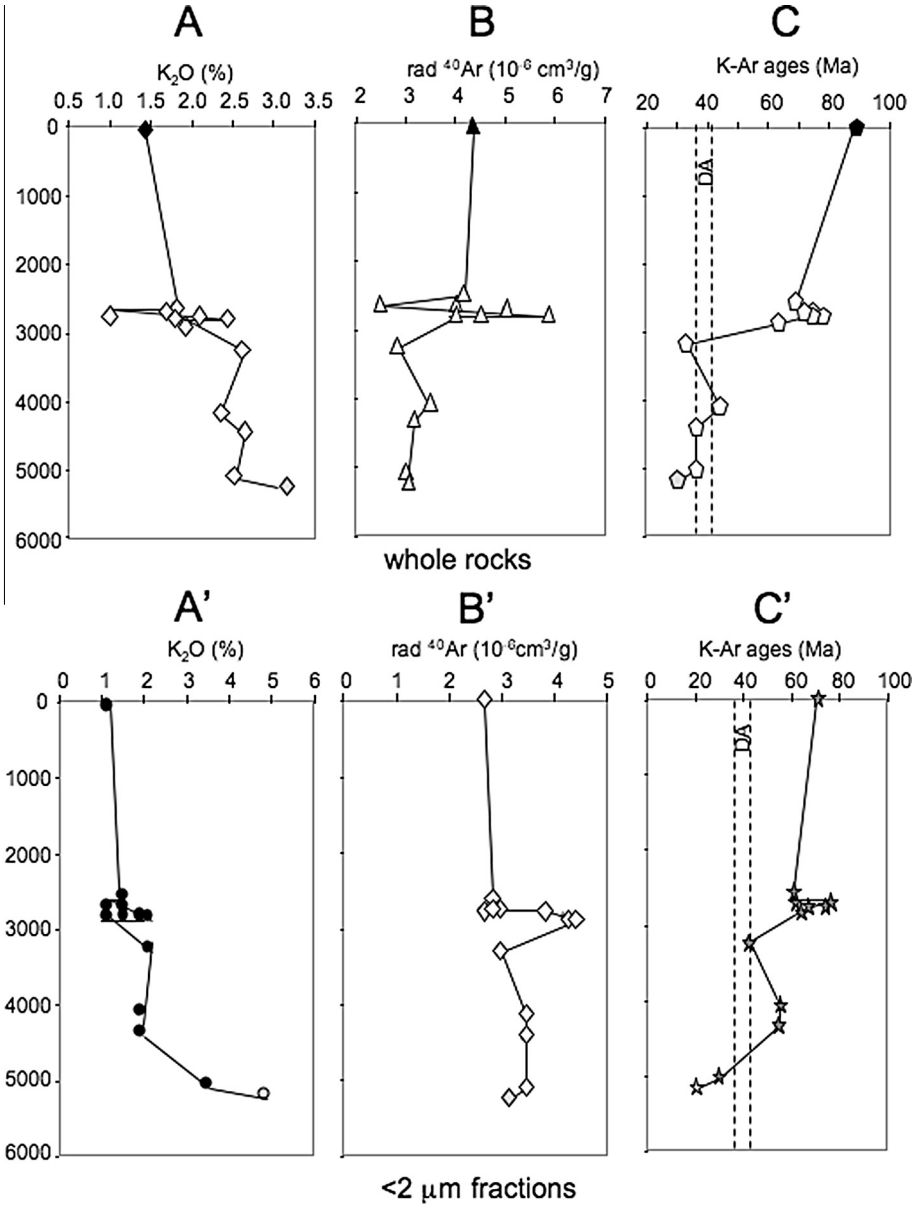

Fig. 2. K_2O and radiogenic ^{40}Ar contents, and resulting K–Ar ages of the naturally matured whole rocks (A, B and C, respectively), and their <2 μm fractions (A′, B′ and C′, respectively). The DA interval denotes range in depositional age according to Johnson and Graham (2007).

3.1.2. The <2 μm fractions

The naturally buried <2 μm fraction consists of I–S, illite, kaolinite, and chlorite (Table 3). Chlorite was only detected in the two deepest N12 and N13 samples. The amount of I–S based on the changing EG patterns (e.g., Brindley, 1980) ranges from 68% in the outcrop N1 sample to 20% in the deepest N13 sample at 5167 m. However, the general decreasing I–S trend shows notable rapid changes between 2585 and 4377 m, with a rapid decrease from 47% to 24% between 2585 and 2828 m in the same well. This rapid decrease is followed by a significant increase to 89% at 3218 m, which is followed by an abrupt decrease to 20% at 5167 m (Fig. 4A). The amount of illite remains fairly constant from outcrop to 2828 m at about 30%, decreases significantly to 10% at 3218 m, and then increases progressively to 43% down to 5167 m (Fig. 4B). Using the calculation by Dolan (1998) based on the Δ2θ method (Moore and Reynolds, 1997), the content of illite layers in the I–S relative to depth is also portrayed here with a fairly constant increase from outcrop to 4093 m, followed by a more rapid decrease to 5167 m (Fig. 4C).

The XRD d_{001} value of the EG-treated samples decreases from 16.71 Å in the outcrop N1 fraction to 13.00 Å in the deepest fraction, which suggests an increase of illite layers in the I–S from 19% to 43% with increasing burial (Table 3). The R0 Reichweite (e.g., degree of

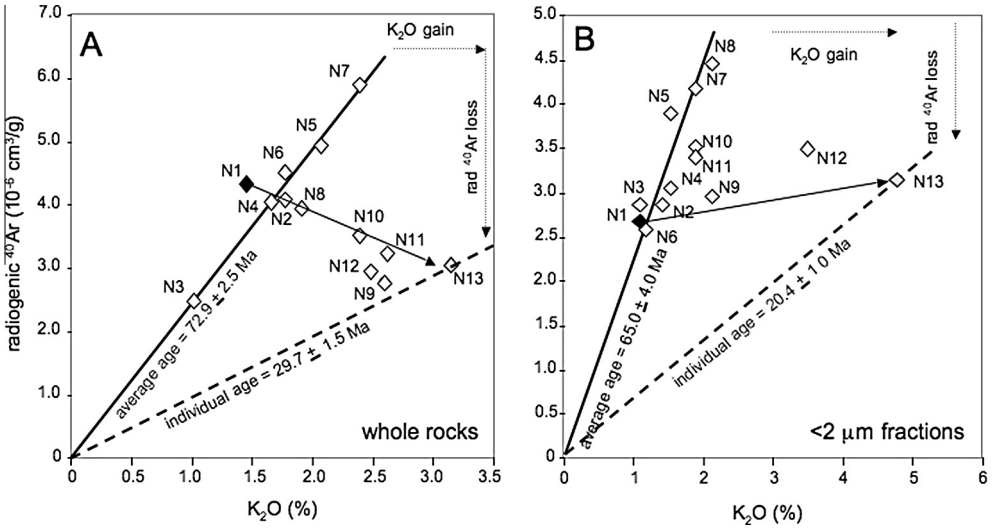

Fig. 3. Harper (1970) diagrams showing the distribution of the radiogenic ^{40}Ar contents relatively to the K_2O contents of the naturally matured whole rocks (A) and their <2 μm fractions (B). Solid line through the origin denotes an equilibrium line for the samples buried to less than 2828 m for the whole rocks with an average age of 72.9 ± 2.5 Ma, and less than 2719 m for the <2 μm fractions with an average age of 65.0 ± 4.0 Ma. The arrow corresponds to the trajectory from less to most mature sample. The dashed line through the origin represents the isochron for the deepest (N13) whole rock with an average age of 29.7 ± 1.5 Ma and its <2 μm fraction with an average age of 20.4 ± 1.0 Ma. Theoretical trajectories for K supply and radiogenic ^{40}Ar release are shown as fine dashed arrows.

ordering of the illite and smectite layers of I–S) identified from surface to 4377 m confirms this content of less than 50% illite layers of the I–S. The R0 Reichweite ordering changes to the R1 type from 5027 to 5318 m with an increased illite content of 60–70%. The Full Width at Half Maximum (FWHM) of the d_{001} illite peak of the AD fractions slightly increases from 0.16 in the outcrop to 0.28 in the deepest sample. The I–S/illite ratio is significantly decreasing with depth from 3.95 to about 1, except for N9 sample at 3218 m. This suggests an overall addition of illite and a concomitant lowering of the I–S amount. In addition to its low content in the outcrop N1 sample, kaolinite amounts are more than 30% at the 2664- to 2761-m interval and at 2828 and 4377 m. As previously mentioned, chlorite is detectable only in the two deepest samples (at 5027 and 5167 m). Except for the 13.00-Å d_{001} value of the EG <2 μm fractions of these two deepest N12 and N13 samples, the d_{001} values range from 16.71 to 18.00 Å with increasing depth. This trend suggests an increasing amount of smectite layers in the I–S in some of the deeper units, contrary to the usual reported downward decreasing smectite trend (e.g., Środoń and Eberl, 1987). The <2 μm fractions also contain some accessory minerals throughout the increasing maturation sequence. The outcrop N1 fraction contains opal-CT, which is not observed in the buried fractions that consistently contain quartz, feldspar(s) and calcite (Table 3).

The summations of the analyzed major elements (Al, Mg, Ca, Fe, Mn, Ti, Na and K) of the <2 μm fraction including the outcrop N1 sample vary from 48 to 116 mg/g (Table 4). The LOI has an overall but irregular tendency to decrease, which is attributed to water loss with increasing illite content and correlative decrease of I–S and its hydrated interlayers. The Al/M ratios of the <2 μm fraction are consistently higher than those of the whole rock, indicating expected higher contents of alumino-silicates, but the overall variations in the trends are generally similar. The Al/Ti ratios remain essentially constant from 21.3 to 26.3, with the exception of a notable increase to 29.3 at 2761 m. The Al/Fe ratio also varies from 1.45 at 2828 m to 4.83 m in the deepest N13 sample at 5167 m. The Al/Ca ratio is also widely varied, similar to that of the whole rocks, which is most probably due to variations in the contents of carbonates. The Al/K ratio of the outcrop N1 sample is similar to that of the two deepest samples with intermediate-depth variations and no systematic trend. The Al/Na ratio is significantly higher in the <2 μm fractions than in the whole rocks, indicating a low abundance of Na-minerals such as feldspars in the <2 μm fractions. Similar to the Al/M trends in the whole rocks, the scatter in the <2 μm fractions indicates significantly different chemical compositions of the original fractions.

K–Ar ages of the <2 μm fraction range from 72.4 ± 4.2 Ma for the outcrop N1 sample to 20.7 ± 0.3 Ma for the most deeply buried N13 sample (Fig. 2). Similar to the ages of the whole rocks, there is an excursion towards older ages from 2585 to 2828 m, and an excursion to a younger age (e.g., 41.9 ± 2.8 Ma) at 3218 m. However, there is no systematic difference between the ages of the whole rocks and those of the <2 μm fractions (Table 2; Fig. 2C and C′), as was observed by Perry (1974) for whole rock ages consistently younger than the 0.5–2 and 2–10 μm fractions of Gulf Coast Miocene shales (Fig. 2C and C′). Similar to the K contents of the whole rocks, that of the <2 μm fraction shows a general increase with depth, with notable variations between 2585 and 2828 m (Fig. 2A and A′). Except for variations between 2585 and 2828 m and a slight decrease between 5027 and 5167 m, the content of radiogenic ^{40}Ar shows only a subtle

Table 3
XRD data on the <2 μm fractions of the naturally matured samples.

Sample designation	Subsurface depth (m)	XRD treat-ment	I–S (% in clay fraction)	I–S d_{001} value (Å)	Δ2θ method illite content in I–S (%)	Reichweite	Illite 9.9–10.2 Å (%)	Illite FWHM (full width at half maximum)	Kaolinite 7.1–7.2 Å (%)	Chlorite 14.2–14.4 Å (%)	I–S/illite ratio	Accessory minerals
N1	0	AD	75	12.84		R0	19	0.16	6	–	3.95	opal-CT + felds.
		EG	68	16.71	8		26	0.16	6	–	2.62	
N2	2585	AD	49	14.64		R0	26	0.20	25	–	1.88	qz. + felds. + calc. + 4.49 Å
		EG	47	16.89	19		29	0.16	24	–	1.62	
N3	2664	AD	34	13.00		R0	34	0.20	32	–	1.00	qz. + felds. + calc. + 4.49 Å
		EG	36	17.09	20		30	0.24	34	–	1.20	
N4	2676	AD	32	14.05		R0	32	0.24	36	–	1.00	qz. + felds. + calc. + 4.49 Å
		EG	33	16.94	17		33	0.24	34	–	1.00	
N5	2719	AD	41	14.84		R0	31	0.32	28	–	1.32	qz. + felds. + calc. + 4.49 Å
		EG	34	17.06	13		33	0.10	33	–	1.03	
N6	2761	AD	26	14.10		R0	37	0.24	37	–	0.70	qz. + felds. + calc. + 4.49 Å
		EG	35	16.89	19		42	0.10	23	–	0.83	
N7	2786	AD	34	14.08		R0	42	0.12	24	–	0.81	qz. + felds. + calc. + 4.49 Å
		EG	29	17.12	17		42	0.20	29	–	0.69	
N8	2828	AD	36	14.03		R0	32	0.16	32	–	1.13	qz. + felds. + calc. + 4.49 Å
		EG	24	16.95	21		32	0.16	44	–	0.75	
N9	3218	AD	86	15.16		R0	10	0.16	4	–	8.60	qz. + felds. + calc. + 4.49 Å
		EG	89	17.18	12		8	0.20	3	–	11.1	
N10	4093	AD	50	12.41		R0	25	0.20	25	–	2.00	qz. + felds. + calc. + 4.49 Å
		EG	71	16.50	16		19	0.12	10	–	3.74	
N11	4377	AD	28	12.00		R0	32	0.12	40	–	0.88	qz. + felds. + calc. + 4.49 Å + trace chlorite
		EG	22	18.00	27		34	0.20	44	–	0.65	
N12	5027	AD	45	11.55		R1	30	0.24	11	14	1.50	overstructure at 38.6 + trace chlorite
		EG	28	13.00	65		39	0.16	15	18	0.72	
N13	5167	AD	39	11.03		R1	33	0.16	14	24	1.18	qz. + felds. + 4.49 Å
		EG	20	13.00	68		43	0.28	19	18	0.46	

I–S stands for illite–smectite mixed layers; AD for air dried; EG for ethylene-glycolated; qz for quartz; felds for feldspars; calc. for calcite; 4.49 Å for unidentified mineral.

increase with depth (Fig. 2B′). The lack of change in ^{40}Ar indicates that addition of K and not release of ^{40}Ar is responsible for the decreasing K–Ar ages, especially in the two deepest samples (Fig. 2C′).

Similar to the whole rocks, the data of the <2 μm fractions at and above 2786 m define an equilibrium line of about 65.0 ± 4.0 Ma in the Harper (1970) diagram (Fig. 3B). These shallow fractions represent the average contents of K and radiogenic ^{40}Ar of the original detrital clay material from uppermost samples. The data points of the <2 μm fractions buried between 3218 and 5027 m plot between the equilibrium line of 65.0 ± 4.0 Ma and the line defining the 20.4 ± 1.0 Ma age of the deepest N13 sample. Similar to the whole rocks, these samples represent different degrees of alteration between the detrital equilibrium line and the deepest and most altered sample. The trend from outcrop N1 fraction to the deepest N13 fraction is again oriented to the right of the diagram with an increasing K content (from 1.12 to 4.77 wt%) and an increasing radiogenic ^{40}Ar content (from 2.69 to 3.16×10^{-6} cm^3/g). The increase of the K content matches the progressive increase of the illite layers in the I–S, except for the N9 and N10 fractions for which K is mostly hosted by illite *sensu stricto* and not by I–S. It is noteworthy that the rapid decrease from 47% to 24% illite in the I–S of the <2 μm fraction between 2585 and 2828 m in the same well is not correlated with a change in the K–Ar ages. This is a result of the K–Ar ages not being solely related to I–S, but rather to mixtures of I–S and discrete detrital and altered illite.

The inability to determine the precise mineral compositions within this depth interval makes it difficult to interpret the cause of variations in the K–Ar ages of the whole rocks. However, in the case of shales, which typically have a high content of clay-mineral sized particles, it is noteworthy to compare the behavior of their K and radiogenic ^{40}Ar contents, and of their K–Ar ages with those of their <2 μm fractions. The general trend of the K content in the whole rocks is continuously increasing with depth, whereas that of their <2 μm fractions abruptly changes from a slow increase to 4377 m followed by a rapid increase at deeper depths. This abrupt change in the trend suggests a significant change in K supply to the authigenic clay material. In both the whole rocks and <2 μm fractions, the K–Ar ages decrease along two successive slopes, gentle in the shallower depths and steeper in the deeper depths. The change in slope is at 2828 m in the whole rocks, and at 4377 m in the <2 μm fractions. It is also noteworthy that the radiogenic ^{40}Ar content slightly decreases in the whole rocks, as it is slightly increasing in the <2 μm fractions. In summary, changes in the K-bearing minerals seem to occur unexpectedly at shallower depths in the whole rocks compared to those in the clay fractions.

3.2. Hydrous pyrolysis maturation

3.2.1. The whole rocks

XRD analysis of the outcrop N1 sample after the pyrolysis experiments shows the same mineral assemblage without significant changes in the non-clay minerals (i.e., quartz, feldspars, opal-CT, and pyrite). The summation of the analyzed elements, excluding the TOC contents, of the outcrop N1 rock and its pyrolyzed aliquots range closely from 120.4 to 141.1 mg/g (Table 5). These elements can be categorized into three groups after pyrolysis: (1) a group with contents above those of the outcrop N1 rock (i.e., Al, Ti and K), (2) a group with contents below those of the outcrop N1 rock (i.e., Fe), and (3) a group with contents below those of the outcrop N1 rock sample after the three initial heating experiments at 270, 290, 310 °C (for 72 h) and above those of the same outcrop N1 rock for the higher-temperature experiments (i.e., Mg, Ca, Mn and Na). The latter group suggests a significant change in the water–mineral-organic reactions around 310 °C. These elements are most likely removed by dissolution in the water phase

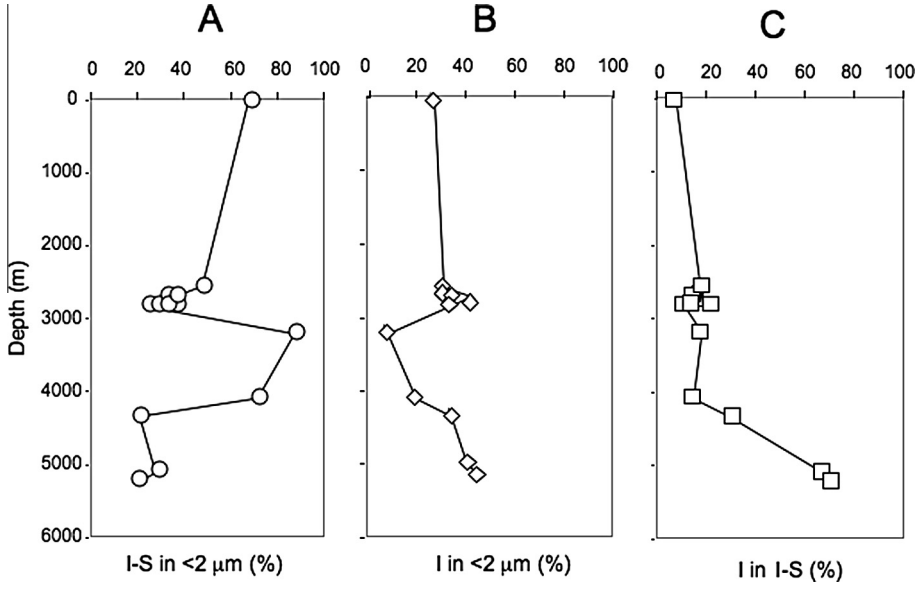

Fig. 4. Measured contents of I–S (A) and illite (B), and modeled content of illite layers in the I–S (C) of the <2 μm fractions from naturally matured rocks.

Table 4
Chemical analysis of selected elements (M), loss on ignition (LOI), and total organic carbon (TOC) of the <2 μm fractions of the naturally matured sequence, and calculated gains and losses based on a conservative Al in the outcrop N1 sample and the naturally matured aliquots according to the method described by Krauskopf (1967) for weathering. The duplicate analysis of outcrop N1 sample is given as a measure of the analytical reproducibility.

Sample designation	Subsurface depth (m)	mg/g <2 μm fraction														
		Al	Mg	Ca	Fe	Mn	Ti	Na	K	Total	LOI (%)	Al/Mg	Al/Ca	Al/Fe	Al/Ti	Al/Na	Al/K
N1	0	64.4	9.10	0.83	28.3	0.121	2.77	1.58	8.78	115.9	22.2	7.08	77.6	2.28	23.2	40.8	7.33
N2	2585	37.5	3.49	4.69	11.3	0.077	1.43	0.65	3.26	62.4	23.8	10.7	8.00	3.32	26.2	57.7	11.5
N3	2664	26.5	2.38	4.35	7.63	0.037	1.07	0.70	2.57	45.2	nd	12.4	6.78	3.87	27.6	42.1	11.5
N4	2676	31.0	3.44	19.0	8.11	0.066	1.35	1.34	3.97	68.3	nd	9.01	1.63	3.82	23.0	23.1	7.80
N5	2719	49.6	4.30	17.7	11.6	0.065	1.91	0.86	3.82	89.9	nd	11.5	2.80	4.28	26.0	57.7	13.0
N6	2761	36.0	5.01	2.87	8.95	0.042	1.23	1.09	2.99	58.2	nd	7.20	12.5	4.02	29.3	33.0	12.0
N7	2786	54.7	5.69	1.10	13.5	0.059	2.08	2.00	4.57	83.7	nd	11.5	49.7	4.05	26.3	27.4	12.0
N8	2828	52.5	7.45	2.15	36.3	0.104	2.04	1.03	5.24	106.8	nd	7.05	24.4	1.45	25.7	51.0	6.50
N9	3218	57.3	5.45	1.70	12.8	0.054	2.33	1.49	8.82	89.9	11.7	10.5	33.7	4.48	24.6	38.5	6.50
N10	4093	56.6	5.50	2.79	14.4	0.079	2.58	1.59	4.71	88.2	18.5	10.3	20.3	3.93	21.9	35.6	12.0
N11	4377	62.2	5.57	1.74	14.2	0.072	2.55	1.33	4.84	92.5	16.0	11.2	35.7	4.38	24.4	46.8	12.9
N12	5027	51.3	5.02	3.76	12.0	0.103	2.41	1.59	5.96	82.1	nd	10.2	13.6	4.28	21.3	32.3	8.61
N13	5167	66.6	5.65	1.92	13.8	0.068	2.41	1.28	9.99	101.7	11.0	11.8	34.7	4.83	27.6	52.0	6.67

LOI stands for loss of ignition and nd for not determined.

during the lower-temperature experiments. Those with increasing contents were retained relative to the initial contents. The summation of the analyzed elements is higher than that of the outcrop N1 sample in all the pyrolyzed rocks at temperatures above 310 °C, which indicates elemental removal of 9.2 to 19.6 wt% of the outcrop N1 rock. These losses can in part be attributed to organic components that were expelled from the rock (i.e., gas, oil and aqueous organic species), as suggested by the decrease in TOC, especially above 310 °C (Table 5).

Unlike the naturally matured rocks that have different original elemental compositions as shown by the Al/M ratios, the pyrolyzed samples do have the same original composition. As a result, elemental gains or losses were calculated assuming Al is conservative as described by Krauskopf (1967; Table 5). With an analytical uncertainty of ±3%, only variations greater than ±6% were considered to be significant. Ti and K are immobile during the pyrolysis experiments with losses between 1% and 5%, and 0–3%, respectively. Na and Mg are slightly mobile with losses between 7% and 8%, and 6–27%, respectively. Ca shows losses at the lower experimental temperatures (⩽330 °C) from 7% to 21%, and gains of 9% at higher temperatures. TOC and Fe show the greatest losses from 23% to 48% and 23% to 36%, respectively. These losses are attributed to expulsion of oil and gas, or mineral dissolution (e.g., Fe) into the interactive water during the experiments.

The K and radiogenic ^{40}Ar contents of the outcrop N1 rock and the pyrolyzed rocks show a slight, stepwise increase with experimental temperature (Table 6; Fig. 5). Rocks pyrolyzed at the three lowest temperatures (270, 290, and 310 °C for 72 h) yield ages that are identical to that of the outcrop N1 sample (89.9 ± 3.9 Ma; Fig. 5C) within analytical uncertainty (93.6 ± 4.4 to 91.6 ± 7.9 Ma). The K–Ar ages of rocks pyrolyzed at the four higher temperatures (330, 343, 349, and 355 °C for 72 h) were younger but essentially constant between (86.8 ± 3.3 and 87.3 ± 3.4 Ma), again within analytical uncertainty with the age of the outcrop N1 sample (89.9 ± 3.9 Ma). At the two highest temperatures (360 and 365 °C for 72 h), the ages were again slightly younger (84.4 ± 4.1 and 85.0 ± 3.3 Ma), but again within the age of the outcrop N1 sample (89.9 ± 3.9 Ma). The sample subjected to the highest thermal maturity (at 365 °C for 216 h) has the youngest experimental age of 75.7 ± 3.4 Ma. These experimental changes in age are significantly less than those observed in the naturally matured rocks (~90 to 30 Ma). This slight decrease in the K–Ar age can be attributed to preferential release of radiogenic ^{40}Ar, as shown in the Harper (1970) diagram (Fig. 6A). The combined changes of K and radiogenic ^{40}Ar in the rocks are strictly reciprocal, with all of the 72-h data points plotting on or near the equi-line defined by the outcrop N1 rock and the pyrolyzed rocks from the four lowest temperatures (P1 through P4; Fig. 6A). The only significant outlier is the P10 sample heated at 365 °C for 212 h.

3.2.2. The <2 μm fraction

The XRD identification of clay minerals in the <2 μm fraction of the outcrop N1 sample and its pyrolyzed ali-

quots is given in Table 7. The I–S content from EG patterns remains about constant between 68% and 63% with a sinusoidal trend that shows no systematic change with increasing experimental temperature (Fig. 7A). The illite content shows a similar trend with increasing experimental temperature between 23% and 32%. The sample heated for 216 h at 365 °C has a higher illite content of 37% (Fig. 7B). The modeled content of illite in I–S (Dolan, 1998; based on Velde and Vasseur, 1992) increases from 5% to 40% with a more marked increase at 270, 290 and 310 °C and essentially no change in the high-temperature experiments (Fig. 7C). The d_{001} value of the AD fractions remains about the same among the outcrop N1 and pyrolyzed fractions from 12.55 to 13.08 Å. The d_{001} value of the EG fractions decreased significantly from 16.71 Å for the outcrop N1 sample to 13.50 Å for the P10 sample, which was heated at 365 °C for 216 h. In addition, the peak at 7 Å in the AD and EG patterns of the outcrop N1 and lowest matured

Table 5
Chemical analysis of selected elements and TOC of the experimentally matured whole rock, and calculated gains and losses based on a conservative Al in the outcrop N1 sample. Percent gains and losses (−) were obtained by calculating the content differences between the outcrop N1 sample and its pyrolyzed aliquots according to the method described by Krauskopf (1967) for weathering. The duplicate analyses on an aliquot of outcrop N1 sample are given as a measure of the analytical reproducibility.

Sample designation	Conditions (°C/h)	mg/g rock								TOC* (wt%)	Total**
		Al	Mg	Ca	Fe	Mn	TiO	Na	K		
N1	Outcrop	60.8	9.91	2.45	27.5	0.223	2.99	5.60	10.9	9.4	120.4
	Duplicate	59.5	9.73	2.09	29.3	0.160	2.88	4.60	10.9	nd	119.2
P1	270/72	68.3	8.19	2.30	21.8	0.154	3.23	5.30	12.1	8.0	121.4
P2	290/72	62.1	8.00	2.01	22.0	0.163	3.00	5.03	11.2	7.5	113.5
P3	310/72	72.2	10.4	2.14	24.1	0.224	3.35	5.70	13.4	6.8	131.5
P4	330/72	72.4	11.0	2.55	21.9	0.233	3.34	5.88	13.0	6.7	130.3
P5	343/72	74.7	11.5	2.83	24.5	0.250	3.61	6.22	13.7	6.4	137.3
P6	349/72	79.0	12.1	3.24	24.8	0.261	3.72	6.93	13.9	6.4	119.2
P9	365/72	75.6	11.3	3.11	27.5	0.281	3.52	6.14	13.6	6.3	141.1
P10	365/216	75.2	11.2	2.77	26.0	0.254	3.52	6.37	13.8	6.3	139.1
		Percent of gains and losses								TOC*	
		Al	Mg	Ca	Fe	Mn	Ti	Na	K		
P1	270/72	0	−27	−11	−32	−29	−3	−8	−2	−26	
P2	290/72	0	−21	−14	−25	−18	−1	−4	0	−23	
P3	310/72	0	−12	−21	−29	−3	−5	−7	2	−40	
P4	330/72	0	−7	−7	−36	1	−5	−4	−1	−41	
P5	343/72	0	−6	0	−31	5	−1	−2	1	−45	
P6	349/72	0	−6	9	−34	4	−3	3	−3	−48	
P9	365/72	0	−8	9	−23	17	−5	−4	−1	−47	
P10	365/216	0	−9	−2	−27	6	−4	0	1	−47	

* The Rock-Eval total organic carbon by USGS.
** Total of the major elements in mg/g; nd stands for not determined.

Table 6
K–Ar data on the experimentally matured outcrop whole rock and its <2 μm fraction.

Sample designation	Pyrolysis conditions (°C/h))	Whole rock				<2 μm fraction			
		K_2O (wt%)	rad. Ar (%)	^{40}Ar rad. (10^{-6} cm^3/g)	Age (Ma) (±2σ)	K_2O (wt%)	rad. Ar (%)	^{40}Ar rad. (10^{-6} cm^3/g)	Age (Ma) (±2σ)
N1	Not heated	1.45	29.98	4.31	89.9 (3.9)	1.13	18.31	2.69	72.4 (4.2)
P1	270/72	1.54	46.44	4.77	93.6 (4.4)	1.10	12.87	2.38	68.8 (4.6)
P2	290/72	1.47	19.00	4.45	91.6 (7.9)	0.98	19.13	2.49	77.2 (4.3)
P3	310/72	1.72	24.88	5.29	93.0 (3.8)	1.03	21.18	2.38	70.4 (5.0)
P4	330/72	1.72	29.62	4.95	87.1 (3.7)	1.18	12.67	2.60	67.2 (6.2)
P5	343/72	1.79	44.03	5.15	87.1 (3.4)	0.86	23.89	2.00	70.7 (5.6)
P6	349/72	1.83	45.43	5.27	87.3 (3.4)	nd	nd	nd	nd
P7	355/72	1.91	52.50	5.47	86.8 (3.3)	nd	nd	nd	nd
P8	360/72	1.66	34.55	4.62	84.4 (4.1)	nd	nd	nd	nd
P9	365/72	1.77	48.82	4.96	85.0 (3.3)	0.84	34.69	1.92	69.7 (4.2)
P10	365/216	1.79	34.98	4.46	75.7 (3.4)	0.89	38.6	1.82	62.4 (3.4)

rad. stands for radiogenic; nd for not determined.

P1 fractions disappears from patterns of the fractions subjected to higher temperatures. This peak is not the d_{002} peak of chlorite, because no peaks are visible at 14 and 7 Å on the H patterns of the outcrop N1 and P1 fractions. With chlorite being absent, this 14-Å shoulder is attributed to the occurrence of expandable smectite-type layers that do not completely collapse by heating as a result of bitumen impregnation of the smectite interlayers (Lewan and Whitney, 1993; Dolan, 1998). Bitumen impregnating the accessible interlayers and coating smectite particle surfaces appears to retard the clay-mineral conversion and minimizes the expulsion of oil generated from partial bitumen decomposition at higher temperatures (> 310 °C). The occurrence of modified organics in the pyrolyzed <2 μm

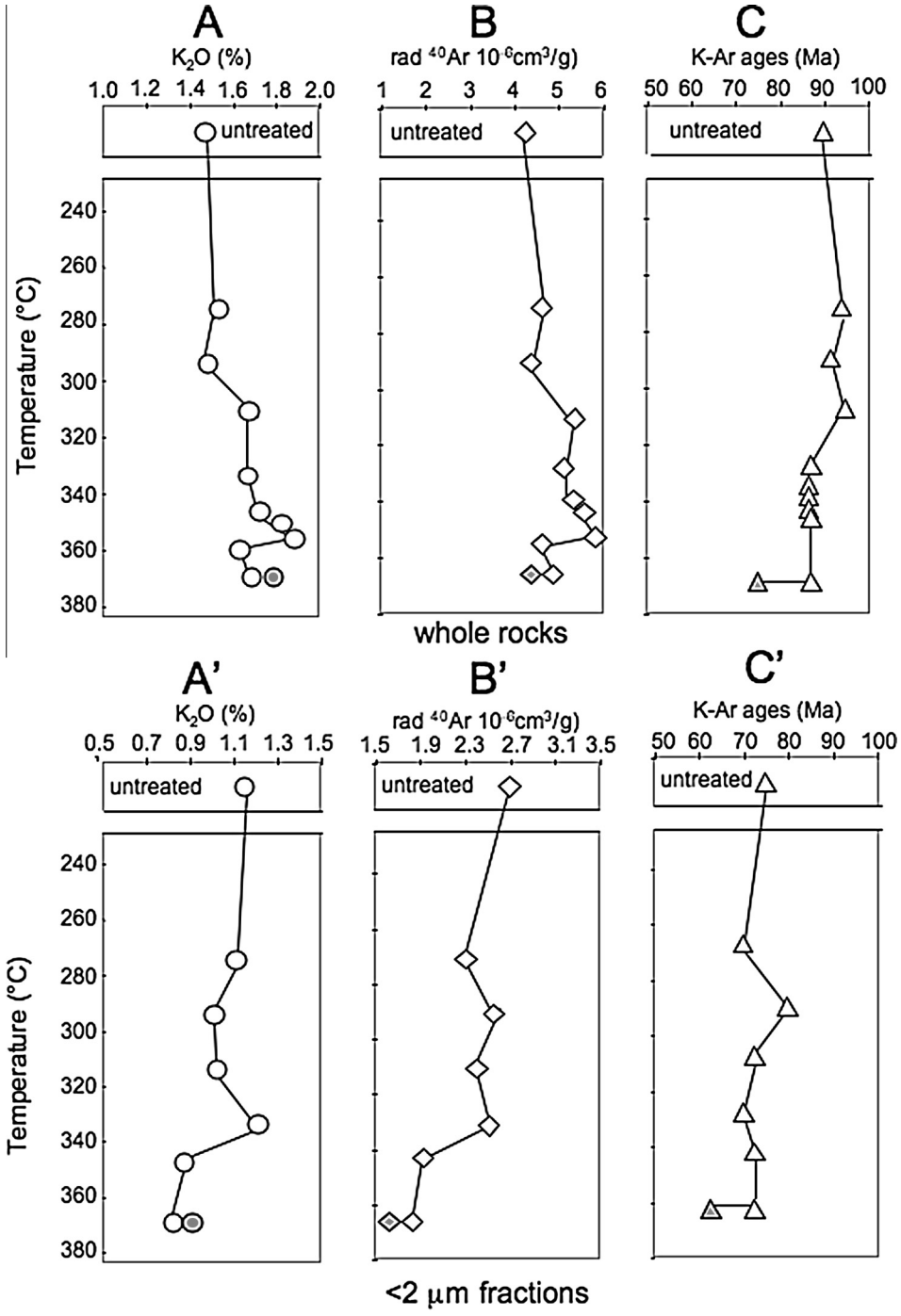

Fig. 5. K_2O and radiogenic ^{40}Ar contents, and correlative K–Ar ages of the experimentally matured rock (A, B and C, respectively), and its <2 μm fraction (A′, B′ and C′, respectively). Experimental temperatures for 72 h are open symbols and the 216-h experiment is a shaded symbol.

fractions is also recognizable by a hump in the background of the XRD patterns between 5 and 3 Å. This hump is not observed in the equivalent XRD patterns of the fractions from naturally matured samples. The study by Clementz (1976) shows that resins and asphaltenes, which are major components of bitumen (Lewan, 1993), can irreversibly enter the smectite-interlayer sites, which reduces layer expandability and increases TOC content.

Clearly recognizable in the P1 and P2 fractions, the R0-type Reichweite ordering of the outcrop N1 fraction is more difficult to identify in the P3 and P4 fractions. The R1-type is observed in the P9 and P10 fractions (Table 7). The illite content remains constant in the I–S from 18% to 24% with 21% for the outcrop N1 fraction. The constant d_{001} values suggest an unaffected mineral with a FWHM increasing from 0.16 in the outcrop N1 fraction to 0.40 in the most mature P10 fraction, which is higher than that determined in the deepest naturally matured sample at 0.28. Kaolinite was detected in the outcrop N1 fraction, but was not identified in the <2 μm fractions of the pyrolyzed rocks (Table 7), which possibly may be a result of its conversion to an amorphous state referred to as metakaolin (Grim, 1968). This transformation has been reported in nature (Spiro, 1979), but it is not a reliable indicator of temperature because of its dependence on the chemistry of associated waters (Dunoyer de Segonzac, 1970). The <2 μm fractions of the outcrop N1 and the pyrolyzed rocks all contain recognizable opal-CT and feldspar as accessory minerals.

The analyzed elements of the <2 μm fractions do not vary significantly during the pyrolysis experiments (Table 8). Similar to the approach used for the whole rocks, Al has been considered conservative during the experiments and used to calculate gains or losses for the other elements. Unlike the whole rock, most of the elements except Ca show some losses in the <2 μm fractions during the pyrolysis experiments. Ca shows the largest gains with values between 54% and 332%, and Fe shows the largest losses between 19% and 47%. Mn also has high gains from 64% to 118%, except in the P1 and P2 experiments. As expected, Ti shows the least change with 7% gains in the experiments up to 310 °C. Na shows systematic losses from 26% to 51%, whereas Mg shows losses of 15% and 17% in the two low-temperature experiments (P1 and P2) and gains from 10% to 21% at the higher experimental temperatures (⩾310 °C). The TOC contents cannot be calculated the same way because its content was not determined in the outcrop N1 fraction. However, there is a general decrease in TOC with increasing experimental temperatures (Table 8). Prior to separation of the <2 μm fraction, Dolan (1998) subjected whole-rock aliquots to the commonly used H_2O_2 treatment for 48 h at 50 °C in order to remove the organic matter and obtain flat and coherent slides for XRD analysis of the <2 μm fractions. Despite this procedure, the <2 μm fractions still contained significant TOC contents, which supports in part the interpretation that the smectite interlayers are unable to fully collapse after heating because of their impregnation with organic matter in the form of bitumen.

The K of the <2 μm fractions decreases in the higher thermal conditions (⩾343 °C), with the exception of an excursion to a higher content at 330 °C (Table 6; Fig. 5A′). The lack of change in K relative to Al suggests that the K-alumino-silicate minerals of the <2 μm fractions remained unaffected by the increasing temperature. Radiogenic ^{40}Ar contents of the <2 μm fractions also show an irregular decrease with temperature increase (Fig. 5B′). The resulting K–Ar ages are about constant between

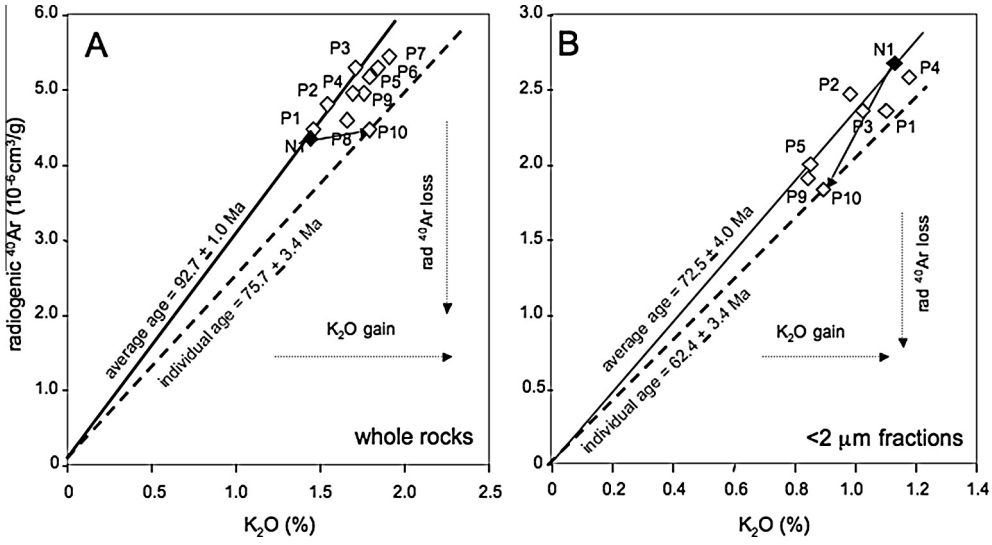

Fig. 6. Harper (1970) diagrams showing the distribution of the radiogenic ^{40}Ar contents relatively to the K_2O contents of the experimentally matured outcropping whole rock (A) and its <2 μm fractions (B). Solid line through the origin denotes an equilibrium line for the samples heated to 310 °C with an average age of 92.7 ± 1.0 Ma for the whole rocks, and to 343 °C for the <2 μm fractions with an average age of 72.4 Ma. The arrow represents the trajectory from less to most mature sample. Dashed line through the origin represents the isochron for the highest maturity whole rock (P10; 365 °C for 216 h) with an average age of 75.7 ± 3.4 Ma and for its <2 μm fraction with an average age of 62.4 ± 3.4 Ma. Theoretical trajectories for K supply and radiogenic ^{40}Ar release are show as fine dashed arrows.

67.2 ± 6.2 Ma and 77.2 ± 4.3 Ma. They remain older than the depositional age and bracket the unheated N1 age of 72.4 ± 4.2 Ma (Fig. 5C′). The youngest age of 62.4 ± 3.4 Ma was obtained after the highest thermal maturity experiment at 365 °C for 216 h. Similar to the whole rocks, the Harper (1970) diagram indicates that the data points of the <2 μm fractions plot around an equilibrium line with a zero intercept for both coordinates (Fig. 6B). The trend from untreated N1 to the pyrolyzed P10 fraction confirms a decreasing content of K and radiogenic ^{40}Ar. In fact, the changes of both the K and radiogenic ^{40}Ar contents are only visible for the two higher-temperature steps at 360 and 365 °C, and their combination has no visible effect on the corresponding K–Ar ages except for the highest thermal-maturity experiment.

4. DISCUSSION

4.1. K–Ar dating of progressively buried whole rocks

K–Ar dating of shale-type whole rocks has generally been discarded because the obtained ages are difficult to relate to varying mineral compositions that outline combined changes in detrital provenance, depositional conditions, and diagenetic alteration. Here, the depositional time is known to be the same for the entire rock sequence. Therefore, the initial detrital K–Ar age of the K-bearing minerals should theoretically be approximately identical at each sampling depth, and variations in the K–Ar ages can help identify changes in the K-bearing mineral assemblage. The progressive decrease of the whole-rock K–Ar ages becomes then an indicator of diagenetic changes in the progressively buried rocks. As a consequence, the K–Ar ages of the deepest samples are younger than the deposition age, and here they indicate a detectable diagenetic impact becoming visible at 3220 m. It is also noteworthy that the rocks above 2800 m contain K-bearing minerals that are of the same origin with about the same age. Decreasing K–Ar ages below this depth result from alteration of the initial detrital minerals, which released K concomitant with crystallization of authigenic material. The K–Ar isotopic budget combines an increasing K with decreasing radiogenic ^{40}Ar. K appears to have been supplied from altered detrital particles of the same rock volume to the crystallizing authigenic phases because no K seems to have been supplied from outside the rocks. This transfer of K from detrital to authigenic minerals is accompanied by an independent release of radiogenic ^{40}Ar. Although the Al/K ratio remains essentially constant, the K content increases through the burial sequence (Fig. 2A). Combination of decreasing K–Ar ages and constant Al/K ratio with depth confirms the internal and limited transfer from detrital to nearby authigenic minerals. The new K-bearing mineral phases crystallizing and growing with burial depth yield more K for the same content of Al, but some scatter remains in the 2664–2828 m interval. This is probably the re-

Table 7
XRD results of the experimentally matured <2 μm fraction.

Sample designation	Pyrolysis conditions (°C/h)	XRD treatment	I–S in <2 μm fraction (%)	I–S d-value (Å)	Modeled illite content in I–S (%)	Reichweite	Illite 9.9–10.0 Å(%)	Illite FWHM	Kaolinite 7.06–7.16 Å (%)	I–S/illite	Accessory minerals
N1	Outcrop	AD	75	12.84	5.0	R0	19	0.16	6	3.95	opal-CT + f elds.
		EG	68	16.71			26	0.16	6	2.62	
		H	sh	–			100	–	nv	–	
P1	270/72	AD	74	12.89	18.0	R0	18	0.24	8	4.11	opal-CT + f elds.
		EG	66	16.50			29	0.20	5	2.28	
		H	sh	–			100	–	nv	–	
P2	290/72	AD	79	13.09	27.0	R0	21	0.20	nv	3.76	opal-CT + f elds.
		EG	77	16.50			23	0.24	nv	3.35	
		H	sh	–			100	–	nv	–	
P3	310/72	AD	72	12.55	36.5	?	18	0.12	nv	4.00	opal-CT + f elds.
		EG	71	14.27			29	0.20	nv	2.45	
		H	30	(11.50)			70	–	nv	–	
P4	330/72	AD	72	12.74	36.5	?	23	0.28	5	3.13	opal-CT + f elds.
		EG	64	14.00			32	0.16	6	2.00	
		H	44	11.98			56	–	nv	–	
P6	349/72	AD	79	12.73	38.0	R1	21	0.24	nv	3.76	opal-CT + f elds.
		EG	75	13.55			25	0.24	nv	3.00	
		H	35	11.74			65	–	nv	–	
P9	365/72	AD	78	12.94	40.0	R1	19	0.28	3	4.11	opal-CT + f elds.
		EG	65	13.60			30	0.28	5	2.17	
		H	71	12.18			29	0.16	nv	–	
P10	365/216	AD	71	12.81	37.5	R1	23	0.36	6	3.09	opal-CT + f elds.
		EG	63	13.50			37	0.40	nv	1.70	
		H	30	12.00			70	–	nv	–	

I–S stands for illite–smectite mixed layers; AD for air dried, EG for ethyleneglycolated, H for heated, ? for difficult identification, nv for not visible, sh for shoulder see text; FWHM for full width at half maximum; felds. for feldspars.

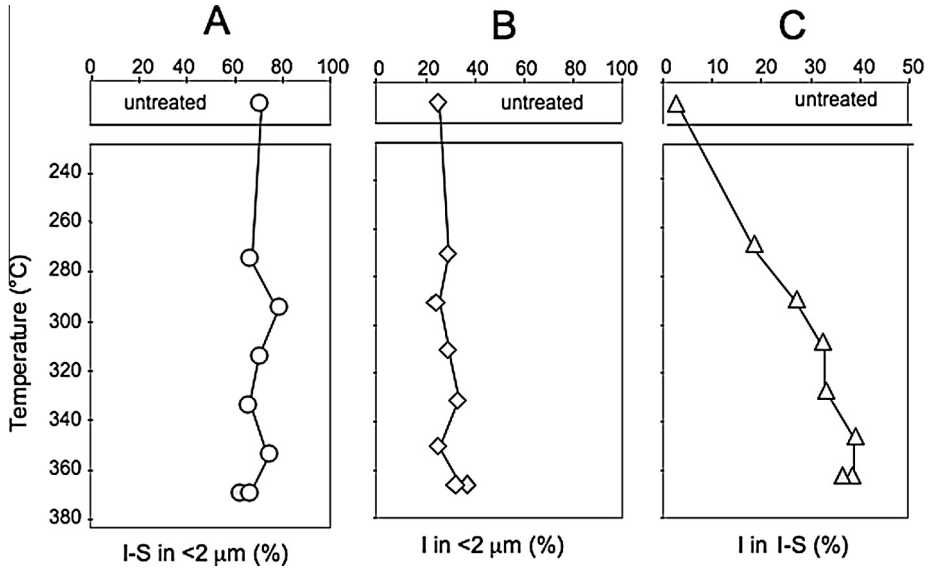

Fig. 7. Measured contents of I–S (A) and illite (B), and modeled content of illite layers in the I–S (C) of the <2 μm fraction from the unheated and experimentally treated whole rock. Experimental temperatures for 72 h are open symbols and the 216-h experiment is a shaded symbol.

Table 8
Chemical analysis of selected elements and TOC of the experimentally matured <2 μm fraction, and calculated gains and losses based on a conservative Al in the outcrop N1 fraction. Percent gains and losses (−) were obtained by calculating the content differences between the outcrop N1 fraction and fractions of its pyrolyzed aliquots according to the method described by Krauskopf (1967) for weathering. The duplicate analysis of outcrop N1 fraction is given as a measure of the analytical reproducibility.

Sample designation	Conditions (°C/h)	mg/g rock								TOC** (wt%)
		Al	Mg	Ca	Fe	Mn	Ti	Na	K	
N1	Not heated*	64.4	9.10	0.83	28.3	0.121	2.77	1.58	8.78	nd
	Duplicate	61.0	10.1	0.88	29.9	0.120	2.65	1.60	9.17	nd
P1	270/72	67.0	8.54	2.04	22.0	0.121	3.10	1.25	8.76	6.3
P2	290/72	65.3	8.53	2.41	19.8	0.129	3.02	0.84	7.25	nd
P3	310/72	66.2	11.3	2.47	17.7	0.277	3.07	0.94	7.89	6.1
P4	330/72	65.4	11.7	3.85	16.0	0.208	2.92	0.81	8.42	5.9
P6	349/72	56.1	10.4	1.89	15.2	0.192	2.53	0.78	6.34	4.9
P9	365/72	57.0	10.1	1.32	16.6	0.207	2.48	0.94	6.80	5.0
P10	365/216	62.1	10.5	1.30	23.4	0.196	2.65	0.86	6.55	4.6
		Percent of gains and losses based on Al content of original N1 sample								
		Al	Mg	Ca	Fe	Mn	Ti	Na	K	
P1	270/72	0	−17	123	−29	−6	7	−26	−9	
P2	290/72	0	−15	171	−35	3	7	−49	−22	
P3	310/72	0	11	174	−42	118	7	−44	−17	
P4	330/72	0	17	332	−47	65	3	−51	−10	
P6	349/72	0	21	147	−42	78	4	−45	−21	
P9	365/72	0	16	70	−37	89	1	−35	−17	
P10	365/216	0	10	54	−19	64	−1	−45	−26	

* Identifies the outcrop sample.
** The Rock-Eval total organic carbon from Dolan (1998); nd stands not determined.

sult of an initial heterogeneity of the detrital mineral phases.

The diagenetic changes in the K-bearing minerals seem to occur unexpectedly at a shallower depth in the whole rocks than in the <2 μm fractions, resulting in decreasing K–Ar ages at shallower depths. If one assumes that clay authigenesis is mainly occurring in the minerals that are of <2 μm size, it can be speculated that the progressively altering detrital K-bearing minerals release their K at a shallower depth than authigenesis of new illite-enriched crystals in the clay-sized mineral fraction. This reasoning is supported by the fact that authigenesis of new K-bearing

minerals need K made available by previous alteration of detrital K-minerals.

In summary, relating K–Ar ages to illitizaton reactions in shales requires a good knowledge of the original overall mineral composition of the deposited subsurface samples. This information is not readily available and caution in interpreting the obtained K–Ar ages should be taken.

4.2. Trends of natural illite, I–S contents, and K–Ar ages relative to burial

Past studies of progressive illitization of I–S and correlative changes in K–Ar ages of naturally maturing sedimentary rocks involved samples that became stratigraphically older with burial (e.g., Perry and Hower, 1970; Perry, 1974; Aronson and Hower, 1976; Clauer et al., 1999). This type of rock sequence is expected to contain material of varying provenance deposited in changing sedimentation conditions. Here, the same rock unit is analyzed from outcrop to various subsurface depths. Although there is no guarantee that the detrital provenance and depositional conditions remained constant regionally over an entire sedimentary basin, the depositional age of the deposited rocks is constrained. Heterogeneity of the original deposited minerals is confirmed by their analyzed elements and their proportionality to Al, which explains the observed changes in mineral, chemical and isotopic compositions with depth in the basin.

The variations in illite and I–S of the <2 μm fractions generally mirror each other in the selected samples, with a decrease in the I–S content from about 70% to 20%, and an increase in the illite content from 25% to 40% with increasing depth. Within the same burial range, the content of illite layers in the I–S increases slowly from 8% at the outcrop to 27% at 4093 m, and then increases rapidly to 80% at 5167 m (Fig. 4C). The K_2O content of the <2 μm fraction increases from about 1.4% to 3.0%, whereas the content of radiogenic ^{40}Ar only increases slightly, resulting in a decrease in the K–Ar ages (Fig. 2C). In fact, the overall content of the K-bearing minerals in the <2 μm fractions that consists of I–S and discrete illite decreases with increasing depth, especially in the deeper section, from 94% at the surface to 63% in the deepest samples. As shown by the linear increase of modeled illite layers in I–S, and by the linear increase of illite content, K was incorporated from the surface outcrop to a depth of about 4093 m, which is also well-marked by the linear decrease in the K–Ar ages above this depth. Below this depth, illitization becomes more intense in the I–S, with a concomitant decrease of the total amount of K-bearing minerals. Noteworthy is the increase of K making the K–Ar ages decrease significantly in the deeper section, below the depositional age. The almost constant amount of radiogenic ^{40}Ar is unexpected.

The overall illite content of the <2 μm outcrop fraction was 26%, increased by 8% illite layers in the 68% of I–S, for a K_2O content of 1.13% and a K–Ar age of 72.4 ± 4.2 Ma. At 5167 m depth, the illite content was of 43% and the illite layers in the I–S was of 80% in the 20% of I–S, for a K_2O content of 4.77% and a K–Ar age of 20.4 ± 1.0 Ma (Tables 2 and 3). The overall illite content of the <2 μm fraction increased from 26% to 60% (by a factor of 2.14) between surface and 5167 m, for an increase of 3.64% (by a factor of 3.22) of K_2O and a decrease of the K–Ar age of 52.0 Ma (by a factor of 3.54). Therefore, K increased more than illite, which indicates that illite layers became enriched in K, reducing the K–Ar ages as the content of radiogenic ^{40}Ar remained essentially constant.

In summary, the results confirm crystallization of authigenic illite, with increased K contents in its interlayers. The results also confirm that the initial detrital illite was altered because the overall K–Ar age is younger than the calculated age of the authigenic illite on the basis of the initial age of the deposited illite.

4.3. Experimental simulation of natural diagenesis

Although K–Ar ages of I–S have been determined on natural buried shales since Weaver and Wampler (1970), no experimental tests to evaluate and simulate the claimed processes have been attempted until this study. The conversion of smectite to illite through the mixed-layer series has been well studied on natural sections (e.g., review by Środoń and Eberl, 1987) and well documented in laboratory experiments (e.g., Huang et al., 1993; Roaldset et al., 1998). However, the balance between K and radiogenic ^{40}Ar used to date the conversion has never been experimentally tested, to the best of our knowledge. Unlike previously reported experimental simulations of the conversion, this study uses a source rock with a high TOC content (9.4 wt%) and oil-prone organic matter (Type-II kerogen), which may have some impact on the behavior of the I–S. In fact, the combined illite and I–S contents of the experimentally matured <2 μm fraction do not change during the experiments, whatever the thermal grade (Fig. 7). Only the modeled illite content in the I–S is significantly increasing up to 310 °C. At higher temperatures, the content remains essentially the same (between 36% and 40%). Because the K content does not increase during the experiments (Fig. 5A), the modeled increase of illite in the I–S most probably corresponds to a partial (35% at the most) collapse of the expandable smectite layers filled with water. Theoretically all smectite layers should have collapsed at the highest temperatures (360 and 365 °C).

Although the modeled amount of illite in I–S (Dolan, 1998) indicates that some mixed layer conversion of smectite to illite occurred in the experiments up to 310 °C, the K–Ar ages show no correlative trend. The sharp but limited decreases in K and radiogenic ^{40}Ar at the highest temperatures (360 and 365 °C) also do not induce significant changes in the K–Ar ages. Therefore, as suggested by Dolan (1998), the failure of smectite to convert to illite may result from a bitumen impregnation of the rock matrix and more specifically a bitumen smearing of the smectite interlayers. The net volume increase in kerogen decomposition to bitumen during the early stages of petroleum formation and hydrous pyrolysis has been shown to transform the rock matrix from a water-wet to a bitumen-wet system (Lewan, 1987). As a result, mineral crystallization and transformation that depend on the occurrence of a water

phase for dissolution and re-precipitation would theoretically be terminated with bitumen impregnation. Therefore, it is not surprising that the smectite to illite conversion is stopped during the experiments, because the bitumen-wet system would hinder K transfer to and radiogenic ^{40}Ar release from the smectite lattice with no younger age emerging from the <2 μm fraction of the rocks. Development of the bitumen-wet system also explains the lack of opal-Ct conversion to quartz, which is also a dissolution and re-precipitation reaction (Rimstidt and Barnes, 1980). Clearly, the high organic-matter content in the Kreyenhagen Shale is probably not suitable to experimentally evaluate K–Ar dating of the smectite conversion to illite. Alternatively, the constant K–Ar ages support the interpretation of the bitumen impregnation of smectite and that kerogen decomposition to bitumen in naturally matured shales inhibits illitization, which also suggests that K–Ar ages of I–S in natural conditions pre-date bitumen formation in source rocks.

Bitumen impregnation of smectite interlayers during hydrous pyrolysis of the Kreyenhagen Shale is also evident by the inability of I–S from the <2 μm fraction to collapse completely upon heating and not fully expanding by ethylene-glycolation at experimental temperatures greater than 310 °C. Bitumen generation during hydrous pyrolysis typically occurs between 300 and 330 °C for 72-h durations (Lewan, 1985). The pyrolysis experiments also indicate that if the amount of bitumen in the rocks and the <2 μm fractions had a tendency to decrease with experimental temperatures (Table 5), some bitumen continued impregnating the smectite interlayers despite increasing temperature, as suggested by the decrease in the amount of ethylene-glycol that normally slips into the smectite interlayer sites (Table 7). In addition to making the interlayer sites unavailable for K, conversion of the water-wet rock matrix to a bitumen-impregnated matrix would inhibit the transfer of K from accompanying feldspars and micas by limiting K diffusion through the bitumen. The retention of bitumen in the smectite interlayers was interpreted as the cause of significant reductions in oil yields from the Kreyenhagen Shale source rock (Lewan and Whitney, 1993; Dolan, 1998).

5. CONCLUSIONS

The thermal maturation of the Eocene Kreyenhagen Shale in the San Joaquin Basin of California was studied by combining mineralogical and chemical analyses with K–Ar dating of progressively buried rocks and their <2 μm fractions. The results are compared with those of a thermally immature outcrop sample and its <2 μm fraction subjected to hydrous pyrolysis. The K–Ar ages decrease from 89.9 ± 3.9 and 72.4 ± 4.2 Ma for the outcrop rock and its <2 μm fraction to 29.7 ± 1.5 and 21.0 ± 0.7 Ma, respectively, in the deepest sample at 5167 m. However, the natural maturation does not provide K–Ar ages in the historical sense, but rather K/Ar ratios of relative amounts of K and radiogenic ^{40}Ar resulting from combined crystallization of authigenic K-bearing mineral phases, and alteration of varied original detrital mineral components of the rocks. Both reactions apparently increase progressively with burial depth.

The Al/K ratio of the naturally matured rocks is essentially constant over the natural maturity sequence, indicating that there is no tendency for a significant K variation relative to depth, and therefore, no supply of K from outside of the rocks. The mineralogical and chemical changes result apparently from recrystallization of carbonates and to a lesser extent from alteration of the K-bearing alumino-silicates within the rock volumes. Conversely, the content of the total organic carbon changed significantly from a low Al/TOC ratio for the immature outcrop sample to higher ratios with increasing burial depth. The initial mineralogy and chemistry of all of the samples and their <2 μm fractions were varied as a result of different depositional settings, but the scattered mineralogy and chemistry progressively homogenized due to increased content of authigenic K-bearing mineral components and increased alteration of the original detrital minerals. Regional variations in the original mineralogy and chemistry of maturing shales can occur as a result of changes in detrital provenance and depositional conditions. As a result, even when the same rock unit is studied at different thermal maturities within a sedimentary basin, variations in the original mineralogy and chemistry of maturing whole rocks challenge the evaluation of the clay mineral transformations, confirming that better information of clay crystals is available from bentonites, especially of nanometric size (Clauer and Lerman, 2012).

With the intent to alleviate the variations in the mineralogy and chemistry of the original rocks from natural maturity sequences within the basin, hydrous-pyrolysis experiments on aliquots of a thermally immature outcrop sample of the Kreyenhagen Shale were conducted to simulate increasing thermal maturation and petroleum formation. The experiments were set at temperatures from 270 to 365 °C for 72 h with one experiment at 365 °C for 216 h. The pyrolyzed rocks and their <2 μm fractions yield a much smaller age range than the naturally buried sequence. K–Ar ages decrease from 89.9 ± 3.9 and 72.4 ± 4.2 Ma for the immature outcrop rock and its <2 μm fraction, respectively, to 75.7 ± 3.4 and 62.4 ± 3.4 Ma at the highest thermally induced maturity (365 °C for 216 h). With K concentrations remaining essentially constant in the pyrolyzed rocks and <2 m fractions, the small change is attributed to smaller losses of radiogenic ^{40}Ar during the experiments than in the natural maturation sequence. The absence of a significant decrease in the K–Ar ages in the experimental maturation sequence as observed in the natural maturation sequence is attributed to the early generation of bitumen, which impregnated the rock matrix and smectite interlayer sites. This resulted in the conversion of the rock matrix from a water-wet system to a bitumen-wet system, which inhibited the availability of K and the precipitation of illite. Future studies to evaluate the smectite to illite conversion should use rocks with low total organic carbon contents (<1 wt%) to ensure that the reaction is not impeded by bitumen impregnation.

ACKNOWLEDGEMENTS

We sincerely thank Zell Peterman of the USGS for his constructive comments on a previous draft, as well as three anonymous reviewers for their focused discussions and questions. Technical contributions of Rob. Wendling, J.L. Cézard, R. Rouault, J. Samuel, Ray. Wendling, R. Winkler and D. Tisserand in Strasbourg are especially appreciated for clay extraction, X-ray diffraction, chemical, and K–Ar isotopic analyses. We also acknowledge S.A. (Tony) Reid at Occidental of Elk Hills, Michael Clark at Arco Western Energy, and Russ Robinson at the California Well Sample Repository for providing samples and helpful advice. Any use of trade, firm, or product names is for descriptive purposes only and does not imply endorsement by the U.S. Government.

REFERENCES

Aronson J. L. and Hower J. (1976) Mechanism of burial metamorphism of argillaceous sediments: 2. Radiogenic argon evidence. *Geol. Soc. Am. Bull.* **87**, 738–744.

Baskin D. K. (1997) Atomic H/C ratio of kerogen as an estimate of thermal maturity and organic matter conversion. *Am. Assoc. Pet. Geol. Bull.* **81**, 1437–1450.

Bonhomme M., Thuizat R., Pinault Y., Clauer N., Wendling R. and Winkler R. (1975). Note Technique de l'Institut de Géologie de Strasbourg, 53 p.

Brindley S. W. (1980) Order–disorder in clay mineral structures. In *Crystal Structures of Clay Minerals and their X-ray identification* (eds. G. W. Brindley and G. Brown), pp. 176–180. Méthode de Datation Potassium–Argon. Appareillage et Technique. Mineralogical Society, London.

Clauer N. (2013) The K–Ar and $^{40}Ar/^{39}Ar$ methods revisited for dating fine-grained K-bearing clay minerals. *Chem. Geol.* **354**, 163–185.

Clauer N. and Chaudhuri S. (1995). *Clays in crustal environments Isotope Dating and Tracing*. Springer Verlag, Heidelberg, 359 p.

Clauer N. and Lerman A. (2012) Thermal history analysis of sedimentary basins: An isotopic approach to illitization. In *Thermal History Analysis of Sedimentary Basins Methods and Case Histories* (eds. N. D. Harris and K. Peters). Society of Economic Petrologists and Mineralogists, pp. 125–146, Special Publication 11.

Clauer N., Rinckenbach T., Weber F., Sommer F., Chaudhuri S. and O'Neil J. R. (1999) Diagenetic evolution of clay minerals in oil-bearing Neogene sandstones and associated shales from Mahakam Delta Basin (Kalimantan, Indonesia). *Am. Assoc. Pet. Geol. Bull.* **83**, 62–87.

Clementz D. M. (1976) Interaction of petroleum heavy ends with montmorillonite. *Clays Clay Miner.* **24**, 312–319.

Czarnecka E. and Gillott J. E. (1980) Formation and characterization of clay complexes with bitumen from Athabasca oil sand. *Clays Clay Miner.* **28**, 197–203.

Dolan M. P. (1998) The role of smectite in petroleum formation: Comparing natural and experimental thermal maturation. Master Degree in Science, Colorado School of Mines, 217 p.

Dunoyer de Segonzac G. (1970) The transformation of clay minerals during diagenesis and low-grade metamorphism: A review. *Sedimentology* **15**, 281–346.

Elzea J. M., Odom I. E. and Miles W. J. (1994) Distinguishing well ordered opal-CT and opal-C from high temperature cristobalite by X-ray diffraction. *Anal. Chim. Acta* **286**, 107–116.

Espitalié J., Madec M. and Tissot B. (1980) Role of mineral matrix in kerogen pyrolysis: Influence on petroleum generation and migration. *Am. Assoc. Pet. Geol. Bull.* **64**, 59–66.

Gavelin S. (1957) Variations in isotopic composition of carbon from metamorphic rocks in northern Sweden and their geological significance. *Geochim. Cosmochim. Acta* **12**, 297–314.

Goldstein T. P. (1983) Geocatalytic reactions in formation and maturation of petroleum. *Am. Assoc. Pet. Geol. Bull.* **67**, 152–159.

Grim R. E. (1968) *Clay Mineralogy*. McGraw-Hill Book Co., New York, 596 p.

Harper C. T. (1970) Graphic solution to the problem of ^{40}Ar loss from metamorphic minerals. *Eclogae Geol. Helv.* **63**, 119–140.

Huang W. L., Longo J. M. and Pevear D. R. (1993) An experimentally driven kinetic model for smectite-to-illite conversion and its use as a geothermometer. *Clays Clay Miner.* **41**, 162–177.

Johns W. D. (1979) Clay mineral catalysis and petroleum generation. *Annu. Rev. Earth Planet. Sci.* **7**, 183–198.

Johnson C. L. and Graham S. A. (2007) Middle Tertiary stratigraphic sequences of the San Joaquin Basin, California. In *Petroleum Systems and Geologic Assessment of Oil and Gas in the San Joaquin Province, California* (ed. A. F. Scheirer). U.S. Geological Survey, p. 18, Professional Paper 1713, Chapter 6.

Krauskopf K. B. (1967) *Introduction to Geochemistry*. McGraw-Hill Book Company, NY, 721 p.

Kübler B. and Goy-Eggenberger D. (2001) La cristallinité de l'illite revisitée: Un bilan des connaissances acquises ces trente dernières années. *Clay Miner.* **36**, 143–157.

Landergren S. (1955) A note on the isotope ratio $^{12}C/^{13}C$ in metamorphosed Alum shale. *Geochim. Cosmochim. Acta* **7**, 240–241.

Lerman A., Ray B. M. and Clauer N. (2007) Radioactive production and diffusional loss of radiogenic ^{40}Ar in clays in relation to its flux to the almosphere. *Chem. Geol.* **243**, 205–224.

Lewan M.D. (1980) Sampling techniques and the effects of weathering: Geochemistry of Vanadium and Nickel in Organic Matter of Sedimentary Rocks. Ph. D., Department of Geology, University of Cincinnati, pp. 47–67.

Lewan M. D. (1983) Effects of thermal maturation on stable organic carbon isotopes as determined by hydrous pyrolysis of Woodford Shale. *Geochim. Cosmochim. Acta* **47**, 1471–1479.

Lewan M. D. (1985) Evaluation of petroleum generation by hydrous pyrolysis experimentation. *Philos. Trans. R. Soc. Lond.* **315**, 123–134.

Lewan M. D. (1987) Petrographic study of primary petroleum migration in the Woodford Shale and related rock units. In *Migration of Hydrocarbons in Sedimentary Basins* (ed. B. Doligez). Editions Technip, Paris, pp. 113–130.

Lewan M. D. (1993) Laboratory simulation of petroleum formation – hydrous pyrolysis. In *Organic Geochemistry, Principals and Applications* (eds. M. Engle and S. Macko). Plenum Press, pp. 419–442.

Lewan M. D. and Whitney G. C. (1993) The inhibitory effect of smectite on petroleum expulsion in hydrous pyrolysis experiments. *Am. Chem. Soc.*, 205th National Meeting, Division of Geochemistry (March 29) Denver, CO. #58 (abstr.).

Lillis P. G. and Magoon L. B. (2007) Petroleum systems of the San Joaquin Basin province, California – Geochemical characteristics of oil types. In *Petroleum Systems and Geological Assessment of Oil and Gas in the San Joaquin Province, California* (ed. A. F. Scheirer). U.S. Geological Survey, p. 52, Professional Paper 1713, Chapter 9.

Lee J. Y., Marti K., Severinghaus J. P., Kawamura K., Yoo H. S., Lee J. B. and Kim J. S. (2006) A redetermination of the isotopic abundances of atmospheric Ar. *Geochim. Cosmochim. Acta* **70**, 4507–4512.

Moore D. M. and Reynolds, Jr., R. C. (1997) *X-ray Diffraction and the Identification and Analysis of Clay Minerals*. Oxford University Press, Oxford, New York, 378 p.

Odin G. S. et al. (1982) Interlaboratory standards for dating purposes. In *Numerical Dating in Stratigraphy* (ed. G. S. Odin). J. Wiley & Sons Ltd, pp. 123–158.

Perry, Jr., E. A. (1974) Diagenesis and K–Ar dating of shales and clay minerals. *Geol. Soc. Am. Bull.* **85**, 827–830.

Perry, Jr., E. A. and Hower J. (1970) Burial diagenesis in Gulf Coast pelitic sediments. *Clays Clay Miner.* **18**, 165–177.

Peters K. E., Pytte M. H., Elam T. D. and Sundaraman P. (1994) Identification of petroleum systems adjacent to the San Andreas fault, California, U. S. A. In *The Petroleum System – From Source to Trap*, vol. 60 (eds. L. B. Magoon and W. G. Dow). American Association of Petroleum Geologists Memoir, pp. 423–436.

Peters K. E., Magoon L. B., Lampe C., Hosford Scheirer A., Lillis P. G. and Gautier D. L. (2007b) A four-dimensional petroleum systems model for the San Joaquin Basin Province, California. In *Petroleum Systems and Geologic Assessment of Oil and Gas in the San Joaquin Province, California* (ed. A. F. Scheirer). U.S. Geological Survey, p. 35, Professional Paper 1713, Chapter 12.

Peters K. E., Magoon L. B., Valin Z. C. and Lillis P. G. (2007a) Source-rock geochemistry of the San Joaquin Basin Province, California. In *Petroleum Systems and Geologic Assessment of Oil and Gas in the San Joaquin Province, California* (ed. A. F. Scheirer). U.S. Geological Survey, p. 102, Professional Paper 1713, Chapter 11.

Pinnavaia T. J. (1983) Intercalated clay catalysis. *Science* **220**(4595), 365–371.

Rimstidt J. D. and Barnes H. L. (1980) The kinetics of silica–water reactions. *Geochim. Cosmochim. Acta* **44**, 1683–1699.

Roaldset E., Wei H. and Grimstad S. (1998) Smectite to illite conversion by hydrous pyrolysis? *Clay Miner.* **33**, 147–158.

Samuel J., Rouault R. and Besnus Y. (1985) Analyse multiélémentaire standardisée des matériaux géologiques en spectrométrie d'émission par plasma à couplage inductif. *Analusis* **13**, 312–317.

Spiro B. (1979) Thermal effects in "oil shales" – Naturally occurring kaolinite and metakaolinite organic associations. *Chem. Geol.* **25**, 67–78.

Środoń J. and Eberl D. D. (1987) Illite. In *Reviews in Mineralogy, 13* (ed. S. W. Bailey). Mineralogical Society of America, Washington, DC, p. 584.

Steiger R. H. and Jäger E. (1977) Subcommision on geochronology: convention on the use of decay constants in geo- and cosmochronology. *Earth Planet. Sci. Lett.* **36**, 359–562.

Tannenbaum E., Huizinga B. J. and Kaplan I. R. (1986) Role of minerals in thermal alteration of organic matter, II: A material balance. *Am. Assoc. Pet. Geol. Bull.* **70**, 1156–1165.

Velde B. and Vasseur G. (1992) Estimation of the diagenetic smectite to illite transformation in time–temperature space. *Am. Mineral.* **77**, 967–976.

Weaver C. E. and Wampler J. M. (1970) K, Ar, illite burial. *Geol. Soc. Am. Bull.* **81**, 3423–3430.

Associate editor: Pete Burnard